

UNIVERSITY OF OKLAHOMA  
GRADUATE COLLEGE

A LOW-LEVEL STABILITY ANALYSIS OF OBSERVED SUPERCELL  
ENVIRONMENTS

A THESIS  
SUBMITTED TO THE GRADUATE FACULTY  
in partial fulfillment of the requirements for the  
Degree of  
MASTER OF SCIENCE IN METEOROLOGY

By

MADELINE DIEDRICHSEN  
Norman, Oklahoma  
2022

A LOW-LEVEL STABILITY ANALYSIS OF OBSERVED SUPERCELL  
ENVIRONMENTS

A THESIS APPROVED FOR THE  
SCHOOL OF METEOROLOGY

BY THE COMMITTEE CONSISTING OF

Dr. Michael Coniglio (Chair)

Dr. Jason Furtado

Dr. Michael Biggerstaff

Dr. Erik Rasmussen



## Acknowledgments

I would like to thank my advisors Dr. Erik Rasmussen and Dr. Mike Coniglio for all of your insight, guidance, and support as I have navigated through classes, research, and field work over the last two years. You have been patient and incredibly supportive through a pandemic that kept our weekly meetings virtual and postponed fieldwork to this spring. I would also like to thank my committee members Dr. Jason Furtado and Dr. Mike Biggerstaff for the helpful feedback, advice, and comments you have made to my thesis. Thank you to my research group who have expanded my perspectives on science and research. I have learned so much from our meetings and am always excited about what questions we can ask and answer next. I would also like to thank all of the people who have made Norman feel like home. From climbing nights, hiking trips, and all of the adventures we've had, I've felt a part of a great community here. And to Sugar, who has sat with me on virtual meetings and classes throughout the pandemic to earn an honorary "meow-teorology" degree. Finally to all of my family and friends who have encouraged my dream and passion for meteorology all these years, thank you for continuing to support me as I have made the move down to Oklahoma.

# Table of Contents

<b>Acknowledgments</b>	<b>iv</b>
<b>List Of Figures</b>	<b>vii</b>
<b>Abstract</b>	<b>ix</b>
<b>1 Introduction</b>	<b>1</b>
1.1 Supercell Environments . . . . .	1
1.2 Sounding Roles in Forecasting Supercells . . . . .	3
1.2.1 Proximity Soundings . . . . .	3
1.2.2 Parameters . . . . .	4
1.3 Background Studies . . . . .	5
<b>2 Data &amp; Methods</b>	<b>9</b>
<b>3 Results</b>	<b>19</b>
3.1 Comparative Regional Analysis . . . . .	22
3.2 Proximity Distributions . . . . .	24
3.2.1 Great Plains . . . . .	25
3.2.2 Southeast U.S. . . . .	27
3.3 Layer Depth Distributions . . . . .	28
3.3.1 Great Plains . . . . .	29
3.3.2 Southeast U.S. . . . .	30
3.4 Thermodynamic Profile Analysis . . . . .	32
<b>4 Discussion</b>	<b>36</b>
4.1 Supercell Environment Variability . . . . .	36
4.2 Supercell Environment Stability . . . . .	38
4.3 Statistical Analysis . . . . .	40
4.3.1 Regional Statistical Significance . . . . .	40
4.3.2 Comparing Tornadoic and Nontornadoic Subsets . . . . .	40
4.4 Comparison of Observed to Simulation Profiles . . . . .	42
<b>5 Conclusion</b>	<b>43</b>
5.1 Summary . . . . .	43
5.2 Future Work . . . . .	46



# List Of Figures

2.1	Distribution of all soundings and the distance launched with respect to the assigned supercell mesocyclone. . . . .	12
2.2	Launch locations of all soundings in the data set, with the Coniglio and Parker (2020) climatology represented by orange dots and the VORTEX-SE data set by navy dots. . . . .	13
2.3	Distribution of sounding launch for a) time of year and b) time of day. . . . .	15
3.1	Kernel Density estimation (KDE) comparing the lapse rate values ( $dT/dz$ ) of all nontornadic (blue contours) and tornadic (red contours) soundings in the data set. . . . .	20
3.2	Box plots depicting low level stability (0-1 km $dT/dz$ ) for each subset: Great Plains tornadic (blue), Great Plains nontornadic (orange), southeast tornadic (green), and Southeast nontornadic (red). The black points represent the lapse rate values of all data points in each subset. . . . .	21
3.3	Histogram for all 0-1 km lapse rates (blue shading) and distribution curves for all 0-1 km lapse rates (light blue line), the Great Plains (orange line), and Southeast (navy line) data sets within a) 0-50 km of the supercell mesocyclone, b) 50-100km, c) 100-150 km, and d)150-200 km. . . . .	23
3.4	Histogram for all lapse rates (blue shading) and distribution curves for all lapse rates (light blue line), the Great Plains (orange line), and Southeast (navy line) data sets within 100 km of supercell updraft in a) 0-100 m, b) 0-250 m, c) 0-1 km, and d)0-3 km layer depths. . . . .	24
3.5	Histogram for all 0-1 km lapse rates (light blue shading) and distribution curves for all 0-1 km lapse rates (light blue line), the Great Plains nontornadic (blue line), and Great Plains tornadic (red line) subsets within a) 0-50 km of the supercell mesocyclone, b) 50-100km, c) 100-150 km, and d)150-200 km. . . . .	26
3.6	Same as Fig. 3.5, but for the Southeast data set. . . . .	28
3.7	Histogram for all lapse rates (light blue shading) and distribution curves for all lapse rates (light blue line), the Great Plains nontornadic (blue line), and Great Plains tornadic (red line) subsets within 100 km of supercell updraft in a) 0-100 m, b) 0-250 m, c) 0-1 km, and d)0-3 km layer depths. . . . .	30
3.8	Same as Fig. 3.7, but for the Southeast data set. . . . .	31
3.9	Averaged potential temperature profile for tornadic (red line) and nontornadic (blue line) environments as well as each respective 25th to 75th percentile (shading). . . . .	32

3.10	Averaged potential temperature profile for tornadic environments (red line), the 25th to 75th percentile of the observed tornadic profile (shading), and the Parker (2012) simulation profiles that intensify vortices: ADIA and A3KM (solid black line) and ALID (dotted black line). . . .	34
3.11	Averaged potential temperature profile for nontornadic environments (blue line), the 25th to 75th percentile of the observed nontornadic profile (shading), and the Parker (2012) simulation profiles that do not intensify vortices: BASE (solid black line), HALF (dashed black line), and B1KM (dotted black line). . . . .	35



## Abstract

Lapse rates have long been used to quantify the stability of the environment and aid in the prediction of storms. Low level lapse rates (0-1 km and 0-3 km) specifically have become a tool in understanding the finer processes that distinguish the environment of tornadic supercells from nontornadic supercells. Several previous studies have attempted to analyze these supercell environments through simulations and case studies though limited regular point soundings near supercells and in the inflow region of supercells have made larger studies more difficult to conduct. The largest dataset of this type to date was analyzed by Coniglio and Parker (2020) who utilized 430 Great Plains supercell inflow soundings from multiple field campaigns over a 25 year period to analyze supercell environments. This study expands the Coniglio and Parker (2020) sounding climatology to include soundings from field campaigns in the Southeastern United States. More than 650 soundings within the inflow regions of 147 supercells were binned by distance from the closest supercell. Then low level lapse rates over different depths and distances were calculated to analyze the stability of tornadic and nontornadic supercell environments. Results show that differences in lapse rate values are statistically significant between the Great Plains and Southeast regions which is expected. Furthermore the 0-100 m near storm environment of tornadic supercells is slightly more stable than that of nontornadic supercells even though there is more variability and that the differences in stability between nontornadic and tornadic supercells decrease with greater distance and sampling depth. The 0-100 m layer in the thermodynamic profile could provide additional insights to the inflow environments of supercells in both the Great Plains and Southeast.

# Chapter 1

## Introduction

In recent years, supercell forecasting has used a combination of ingredients (moisture, lift, instability, and shear) and parameter (e.g. SRH, LI, SCP, etc) based input from models, satellites, National Weather Service (NWS) soundings, and other observations. These forecasting tools have aided in the improvement of predicting supercells as well as tornadoes, but there is still a need for understanding the mesoscale and storm-scale difference between tornadic and nontornadic supercell inflow environments. This has been addressed in recent simulation experiments, case studies, and observed climatologies that have aimed to find differences in the kinematic and thermodynamic profile of the supercell environment. The remainder of the introduction reviews supercell characteristics and convective environments in the Great Plains compared to the Southeast United States, how sounding data are used in forecasting, and how past studies have used soundings to analyze low-level supercell environments.

### 1.1 Supercell Environments

Supercells have long been defined as a storm with a persistent rotating updraft known as a mesocyclone (e.g., Rotunno and Klemp, 1984; Markowski and Richardson, 2010). Supercells differ from other storms because they rotate, propagate away from the mean wind vector, and are most likely to produce tornadoes and significant severe weather. A supercell's environment is usually classified by an inflow region downshear from the

main rotating updraft which is located between a forward flank downdraft and a rear flank downdraft (Davies-Jones, 2015). The rear flank downdraft, forward flank downdraft, and inflow regions are important in tornadogenesis. The forward flank downdraft provides streamwise vorticity that wraps around with the rear flank downdraft and eventually tilts into the updraft while supercell continues to ingest warm moist air from the inflow region (Markowski and Richardson, 2010). The inflow environment can also be modified by the storm itself by anvil shading (Nowotarski and Markowski, 2016) and other processes. It is important to understand the mesoscale processes associated with supercells both kinematically and thermodynamically as substantial evolution can occur on the order of minutes.

Many past studies and conceptual models have been based on Great Plains events as the environments in the Great Plains favor discrete supercells in locations where data can be collected (e.g., Rasmussen and Blanchard, 1998; Parker, 2014, 2021). These environments surrounding the supercells are marked by nearly dry adiabatic lapse rates, large instability, and strong wind shear which combined increase the likelihood for discrete storms. These variable also increase the potential for hazards such as large hail, strong straight-line winds, and tornadoes.

The focus of Southeast United States (hereafter shortened to Southeast) studies has largely been on quasi-linear convective system (QLCS) environments, but supercells still make an impact in the region (Bunkers et al., 2006; Murphy and Knupp, 2013; Chasteen and Koch, 2022). Since convective mode is largely controlled by the orientation of the shear vector to the boundary of convection initiation (Thompson et al., 2012), the thermodynamic environment can be assumed to be similar for convective events with mixed mode convection (supercells, clusters, and QLCS). These inflow environments are commonly marked by high shear and low CAPE profiles (Guyer and Dean, 2010; Sherburn and Parker, 2014; Anderson-Frey et al., 2019; Wade and Parker,

2021) which differ from the high CAPE convective environments common across the Great Plains. The low CAPE scenario is caused by increased cloud cover and cooler surface temperatures which also decreases low level lapse rates (Schneider et al., 2006). Supercells tend to develop in messier environments in the Southeast than their Great Plains counterparts with the potential for clustered cells, embedded supercells, and stratiform precipitation surrounding the supercells. The differences in Southeast and Great Plains supercell environments are rooted in the amount of moisture available in the environment, the surface temperatures, mixed layers aloft, and most importantly buoyant energy during convective events.

## **1.2 Sounding Roles in Forecasting Supercells**

### **1.2.1 Proximity Soundings**

Proximity soundings have held various definitions throughout literature (e.g. Showalter and Fulks, 1943; Maddox, 1976; Wade et al., 2018), each based on the criteria of the data set analyzed. For example, the proximity distance threshold ranged 50 miles from an observed tornado in Beebe (1958) to 400 km in Rasmussen and Blanchard (1998). Even with these point differences, all definitions kept a few ideas in common: the sonde should be launched within a certain distance of a target feature, the sonde should be launched within a specified amount of time from when the feature was observed, and all sondes should be launched within a representative environment. Potvin et al. (2010) defined proximity criteria best as a way to provide a representative sample of a targeted storm environment. To define the proximity area for a supercell environment, the extent of the modified environment to the surrounding homogeneous environment would need to be estimated. This can be very difficult to pinpoint when analyzing mesoscale

and storm-scale processes and therefore studies have selected proximity definitions that encompasses the data set and research goals of each study.

### 1.2.2 Parameters

Over the years, parameters derived from environmental variables have been developed and used to forecast supercells (Rasmussen and Blanchard, 1998; Rasmussen, 2003; Thompson et al., 2007). Kinematic parameters calculate the difference in wind speed and direction with height (i.e. bulk shear, storm-relative helicity (SRH), and vertical vorticity). There are also thermodynamic parameters such as convective available potential energy (CAPE), lapse rates, lifting condensation level (LCL), convective inhibition (CINH), and more that characterize aspects of the storm environment in relation to convective instability and buoyancy of a specified profile. These parameters are often relied on in supercell forecasting as they encompass the four ingredients required for supercells: lift, instability, moisture, and shear (Markowski and Richardson, 2010). Greater amounts of instability (higher values of CAPE and steeper lapse rates), wind shear (higher values of bulk shear and SRH), moisture (lower LCLs), and a source of lift all result in an environment favorable for supercells. Kinematic variables such as bulk shear tend to be the focus of studies comparing tornadic and nontornadic environments (e.g., Coffey and Parker, 2017, 2018; Coniglio and Parker, 2020) since the formation and sustainability of tornadoes is thought to rely on wind shear and streamwise vorticity. The thermodynamic profiles of nontornadic and tornadic supercell environments has been studied much less even though the amount of instability in the inflow parcels, surface temperatures, and even LCL heights also play a role in tornadogenesis. Both the thermodynamic and kinematic profiles of supercells need to be examined to determine factors influencing tornadogenesis.

### 1.3 Background Studies

Several observational studies have analyzed the low level thermodynamic environment of nontornadic and tornadic supercells observed by radar and proximity soundings. Wade et al. (2018) selected 28 sounding pairs from the Mesoscale Predictability Experiment (MPEX), MiniMPEX, and second Verification of the Origins of Rotations in Tornadoes Experiment (VORTEX2) field campaigns, 12 of which were launched in tornadic supercell environments and 16 launched in nontornadic supercell environments. Each of these sounding pairs consisted of a near-field and far-field sounding within the inflow environment of each supercell thunderstorm. Greater cooling and moistening above the boundary layer was evident in the near-field of the nontornadic supercell environment than the tornadic environment. A near surface statically stable layer was found to only be present in the near-field nontornadic soundings. The study asserted this result could be due to anvil shading or a manifestation of near surface instrument errors. In an earlier study, Parker (2014) analyzed composite environments from 134 soundings launched during VORTEX2. The soundings were selected from both the inflow and outflow environments of supercell thunderstorms within 100 km of the mesocyclone. This study showed that temperatures cool by 0.5 to 1 K in the near field, potentially owing to the effects of anvil or other cloud shading. Meanwhile, a slight moistening and warming aloft in the tornadic profiles was found which may act to lower lapse rates in the column. Kinematically there was an increase in low-level wind shear from far-field to near-field in the nontornadic supercell environments, but the low-level wind shear was greater and constant across the inflow region of the tornadic supercell environments.

In the largest sounding climatology to date, Coniglio and Parker (2020) compiled a data set of over 600 soundings from nontornadic and tornadic supercell events during a

25 year period (1994-2019) of field campaigns. In each of these events they defined the inflow region of a target supercell as -130 to 40 degrees in azimuth from the updraft. These angles allowed for the soundings to reside in the most likely rain free environment ahead downstream of the mesocyclone. The soundings selected were all launched within 160 km of the defined mesocyclone with a separation between near-field soundings (10-40 km) and far-field soundings (40-100 km). The soundings were quality controlled by manually analyzing each near surface profile and removing suspect thermodynamic and kinematic observations. Soundings with negative 0-3 km CAPE and thermodynamic characteristics of being launched in outflow winds were excluded from the data set, leaving 430 proximity soundings to be analyzed.

Once the climatology was finalized, the soundings were classified as tornadic or nontornadic and given an Enhanced Fujita scale rating if a tornadic flag. Multiple kinematic and thermodynamic parameters were analyzed and compared between the nontornadic and tornadic soundings as well as the near and far-field inflow environments. The main findings focused on the kinematic parameters, but one of the surprising thermodynamic findings showed that the average lapse rate of the tornadic soundings was 2 K/km lower than the average lapse rate of the nontornadic soundings in the 0-100 m and 0-250 m layers. While 2 K/km is a substantial difference in lapse rates, the value was found to not be statistically significant.

Studies have also relied on both simulations and observed soundings to examine how environmental variables influence vortex intensification. Both Coffey and Parker (2017) and Coffey and Parker (2018) simulated nontornadic and tornadic near-storm environments from VORTEX2 observed soundings to determine what storm-scale processes may cause tornadogenesis. The studies utilized composite soundings from Parker (2014) as a base state to focus on the influence of low-level wind profiles. The amount

of streamwise vorticity being stretched into the low-level mesocyclone had the greatest influence on whether a vortex intensified in a simulated storm (Coffer and Parker, 2017). Coffer and Parker (2018) also noted that the input thermodynamic and kinematic environment composites slightly influenced the potential of a simulated storm to become tornadic. Parker (2012) focused solely on the thermodynamic profile of simulated environments to determine if dry adiabatic lapse rates result in vortex intensification. The study introduced six individual vertical potential temperature profiles with changes of potential temperature lapse rates at 1 km, 3km, and 10 km as the rest of the parameters for the model were held constant. The three profiles that kept a constant potential temperature (dry adiabatic lapse rate) in the first kilometer led to vortex intensification, while the three profiles characterized by 0-1 km subadiabatic lapse rates did not produce a vortex.

Each of the observed and simulation studies highlighted the stability of the low-level thermodynamic profile, but did not reach the same conclusions. The larger lapse rates in the near surface tornadic composites in Wade et al. (2018) contradict the findings from Coniglio and Parker (2020) who had found that the 0-100 m and 0-250 m lapse rates were lower for tornadic soundings than nontornadic ones. Parker (2012) findings agree with the Wade et al. (2018) as the 0-1 km lapse rates of simulated vortex profiles were larger than the the base lapse rates. On the other hand, Parker (2014) findings agrees with Coniglio and Parker (2020) where boundary layer lapse rates are lower for tornadic environments than nontornadic environments. Differences in proximity thresholds, depth of the layer analyzed, and the sample size of the data sets may have led to the contradictory findings of these studies. The first goal of this study aimed to answer these contradictions by expanding Coniglio and Parker (2020) climatology with Southeast soundings to subjectively and objectively analyze the low-level lapse rates of both nontornadic and tornadic supercell inflow environments. By increasing



the data set size and analyzing soundings at set binned ranges from the supercells and at binned depths in the near-field environment, this study determined the differences in the low-level thermodynamic environment of tornadic and nontornadic supercells.

The defined simulation profiles from Parker (2012) led to a another avenue of exploration regarding low-level thermodynamic environments. The second goal of this study was to determine if simulation thermodynamic profiles developed by Parker are present in observed environments and if those profiles are associated with the same outcomes (e.g. tornadic or nontornadic) as the observed environments. If so, there are a significant difference between tornadic and nontornadic thermodynamic profiles. If not, then the profiles used in the simulation are not representative of observed supercell environments.

## Chapter 2

### Data & Methods

This study used and expanded upon the Coniglio and Parker (2020) sounding data set by initially adding over 200 soundings and cases collected during the VORTEX-SE field campaigns from 2016-2019, including the MESO 18-19 field campaign, that met the criteria for the Coniglio and Parker study as described below. All sounding instruments used in the VORTEX-SE data set were either Vaisala Radiosondes (R92), Sparv Windsonds, iMet-4, or Lockheed Martin Sippican LMS-6 launched at semi-fixed sites in Alabama, Mississippi, Louisiana, and Florida. National Weather Service offices also launched special soundings at 06z and 18z on specified days during each field campaign. Once the events containing supercells were identified in the VORTEX-SE data set, a quality control of the soundings, radar analysis of storm location, assignment of soundings, and defining tornadic soundings could then be conducted using the Coniglio and Parker (2020) approach.

Since multiple sounding platforms were used to compile the data set, special care was taken to address each platform's biases and quality control the soundings further as needed. Coniglio and Parker (2020) addressed the dry bias of Vaisala RS80 sondes by increasing RH as a function of height derived from Wang et al. (2002). In addition, the surface data points of Sparv Windsonds were corrected for altitude and temperature errors that accumulated as the windsonds were frequently turned on minutes before launch in air conditioned vehicles. Assigning the surface values to the data points

directly after the sonde began to ascend accounted for both the altitude and temperature errors. Once these known specific platform biases were corrected, each of the soundings were quality controlled following the Coniglio and Parker (2020) approach. All low-level lapse rates assumed 20 m as the first data point of the layer to account for potential surface temperature and relative humidity discrepancies with the sonde temperature and relative humidity near the ground that arise from using a separate system (mobile mesonet) for surface conditions. As with Coniglio and Parker (2020), all sounding fields were linearly interpolated to 10 m levels throughout the profile and, when calculating the lapse rates in each layer, an observed data point was required to reside within 50 m of the requested level.

Supercells were then manually identified for each event and analyzed using WSR-88D data in GR2 Analyst. Both base level reflectivity and velocity from the closest WSR-88D radar were used to track the mesocyclone location of the main supercell up-draft throughout the storm's life cycle which was defined from first echo to dissipation or merged with other cells (Coniglio and Parker, 2020). Each storm was required to have either a rotation couplet visible on velocity or an inflow notch shape detectable in reflectivity in each scan for at least one hour to be labeled as a target supercell. Unlike past studies, a threshold of maintaining supercell characteristics for at least 60 minutes was required because a base azimuthal shear value was not set. Storm motion vectors were then determined by manually selecting the location of the mesocyclone at each scan, then deriving the instantaneous speed and direction at each point by compiling a five-scan weighted average and averaging the three closest speeds to the sounding launch time (Coniglio and Parker, 2020).

Once each supercell was identified and the storm speed calculated, the soundings were assigned to a storm based on the following criteria: the sounding was located between -130 to 40 degrees in azimuth to the storm and the storm was the closest

supercell to the sounding at time of launch (in the case there were multiple supercells). Therefore each sounding was assigned to one storm, but each storm had the potential for multiple soundings to be launched in the inflow region. While the sounding environments are not strictly independent from one another, this allows for the changing environment in the lifetime of a storm to be considered and analyzed.

Supercells were also classified as tornadic and nontornadic at each radar scan using reports from the SPC "one-tor" database (Smith et al., 2012). Following the Coniglio and Parker (2020) approach, a flag was added at each scan of the storm if a tornado was reported at the beginning of the scan and if so, the EF-scale rating that was added to the database afterwards. The EF-scale rating was assigned a singular value corresponding to the maximum assigned wind speed of the tornado. While tornado intensity was not analyzed in this study, future work may address the tornado strength at the closest point to when the sonde was launched. For the purpose of this work, the soundings were each labelled as nontornadic or tornadic. This was done by determining whether the supercell assigned to the sounding was flagged as tornadic as a time six minutes prior to ninety minutes after the sonde was launched.

A proximity definition used by Coniglio and Parker (2020) was initially applied to the data set, where a threshold of 160 km between the launch location and target supercells was used. This distance captured a large portion of the Great Plains data set, but excluded a greater number of Southeast soundings launched at fixed locations, usually farther from the target supercells. In order to increase the number of soundings from the Southeast events, the proximity distance was expanded to 200 km. This added 23 soundings as shown in Fig. 2.1 and increased the Southeast data set by twenty percent. This also allowed for a 50 km bin size when comparing supercell environments at different distances. In addition, expanding the data set increased the

likelihood that a controlled environment outside of the supercell proximity region could be compared to the environments sampled closer to the supercells.

Distribution of each Sounding Distances from Respective Storm (Bin size = 10 km)

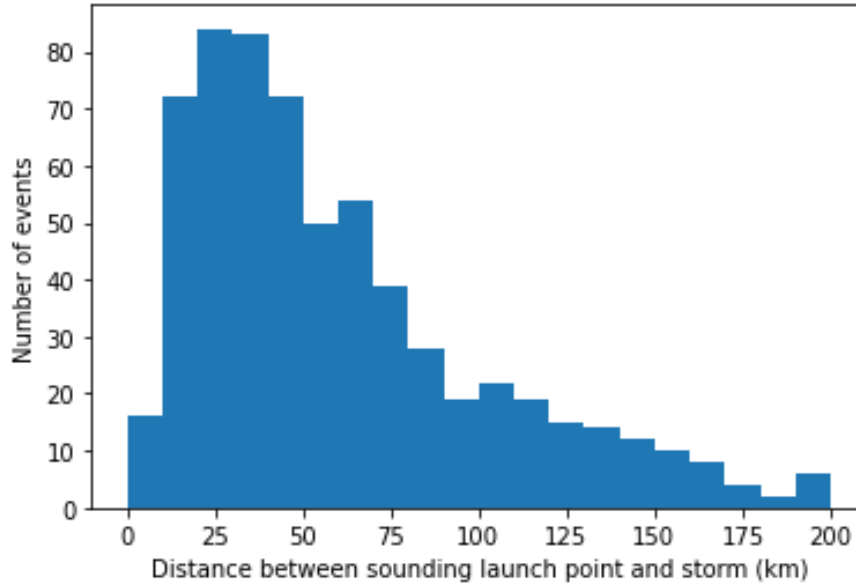


Figure 2.1: Distribution of all soundings and the distance launched with respect to the assigned supercell mesocyclone.

After quality controlling the soundings and defining the distance and proximity thresholds, a total of 667 soundings were selected for this study. Fig. 2.2 shows each launch site location with the Coniglio and Parker (2020) data set highlighted in orange (587 soundings) and VORTEX-SE data set highlighted in navy (83 soundings). The number of sondes launched in the Great Plains was five times greater than those launched in the Southeast due to a longer collection period (twenty-five years compared to four years) and because supercells have not been the main convective mode target for Southeast field campaigns in the past. The smaller sample size of the Southeast data set led to less robust results, but including the geographical region in this study

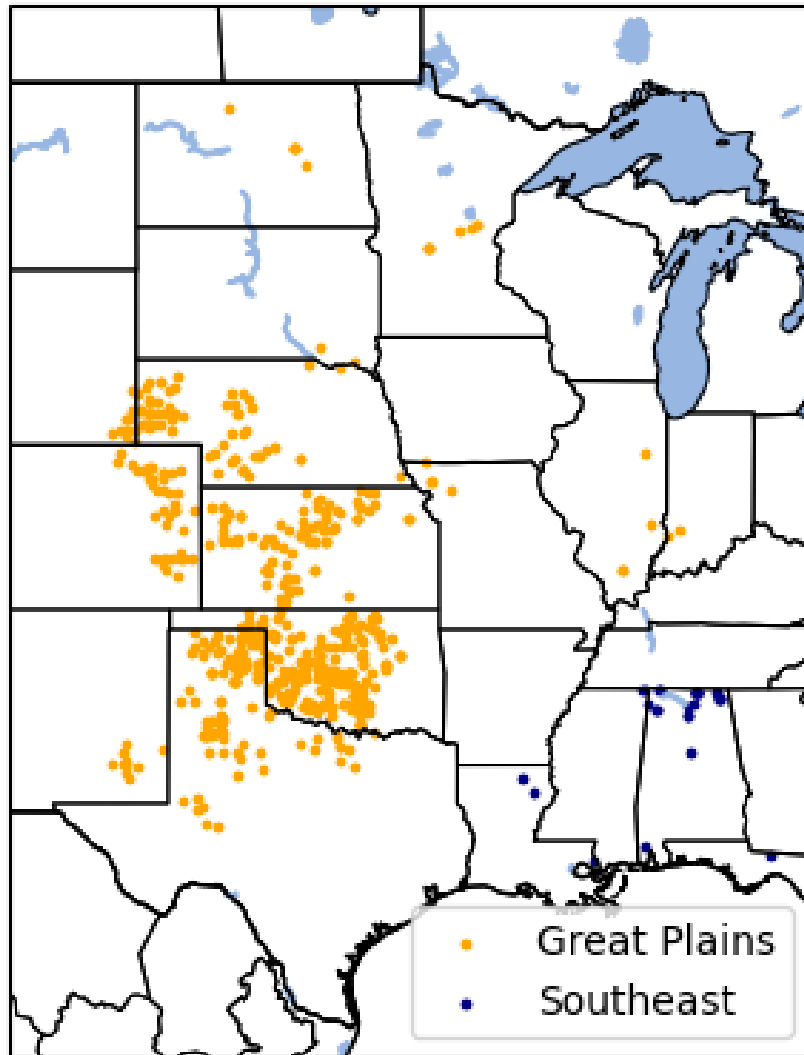


Figure 2.2: Launch locations of all soundings in the data set, with the Coniglio and Parker (2020) climatology represented by orange dots and the VORTEX-SE data set by navy dots.

was imperative in order to expand our knowledge of Southeast supercell environments from observed soundings to benefit future Southeast convective studies.

Another difference between the Southeast and Great Plains data sets was the annual and diurnal timing of the launches. The Great Plains soundings were all launched in the months of April, May, June, and July. As shown in Fig. 2.3, additional soundings were launched in November, February, and March. These, along with a small number in April, were collected during VORTEX-SE field campaigns. The cold season events that occurred in November, February, and March were considered in analyzing the environments of Southeast soundings in the study. The diurnal timing of sounding launches also shown in Fig. 2.3 are consistent with the typical diurnal variations in convection. The outliers between 10 to 14 UTC in Fig. 2.3 were launched during two VORTEX-SE events targeting overnight convection and supercells. The thermodynamic profile of these soundings were slightly more stable within the lowest 1 km, but did not substantially change the results of the analysis.

One important consideration when interpreting the results of this study is the representativeness of using soundings to classify a storm environment. Soundings generate a time series of point observations that only sample the atmosphere that is transected by the sonde. This means that heterogeneities and other rapidly evolving environments could potentially be missed if the sonde does not transect it, or alternatively, that a sonde that passes through a local-scale feature (e.g. a horizontal convective roll; Weckwerth et al. (1996)) may not represent the larger-scale environment within which the storm resides. These sources of error are unavoidable when using single sonde, or a small number of sondes, per event. Past studies have utilized composites, self organizing maps, and other ways to average sounding data points in an attempt to characterize the entire supercell inflow environment but in doing so also removed signals such as thermodynamic gradients. Modelling soundings on a gridded system has made it easier to create averaged maps, but it has been impossible to compile enough observed

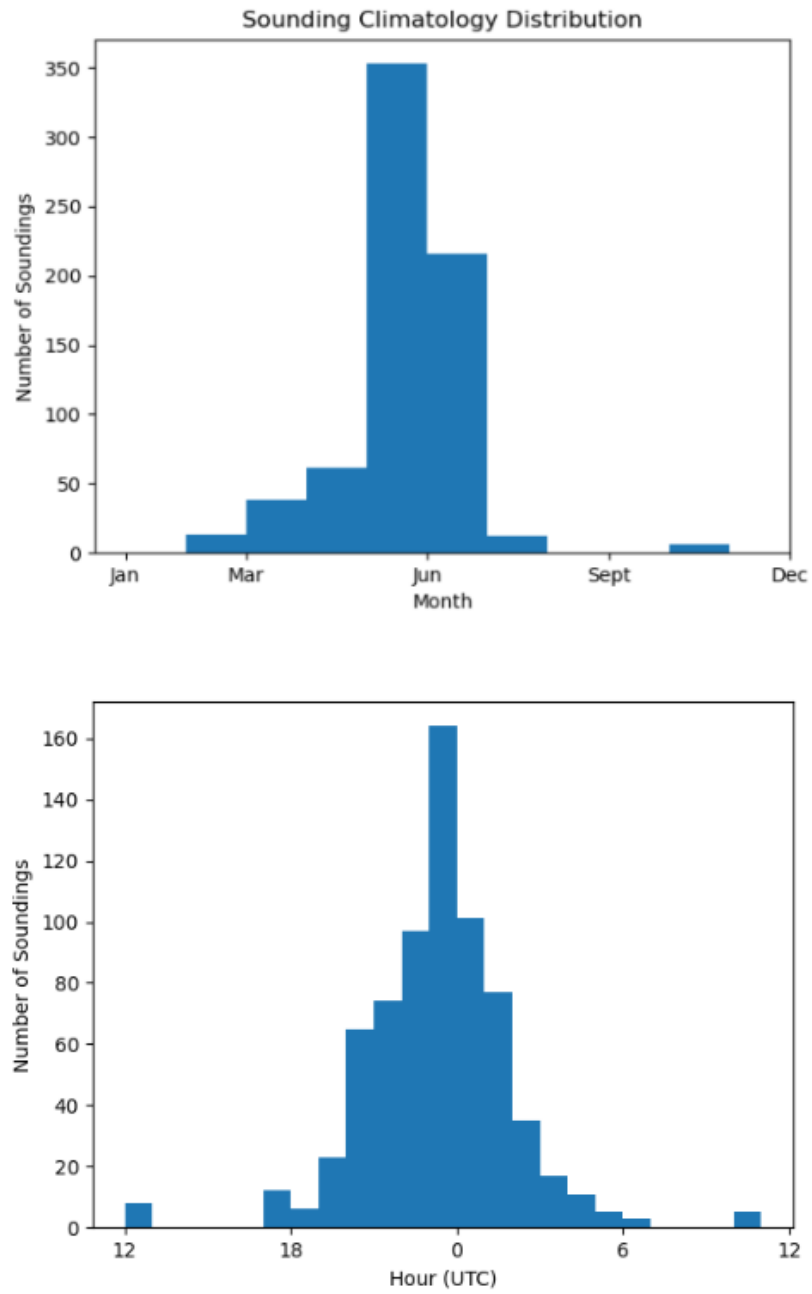


Figure 2.3: Distribution of sounding launch for a) time of year and b) time of day.



soundings in supercell environments to be representative of the entire environment. This study took the approach of analyzing a large data set of observed soundings from twenty-five years of field campaigns that is assumed to contain unbiased representativeness errors across the data set. In an attempt to capture inhomogeneities across typical supercell environments, the soundings were binned with respect to distance to the supercell updraft and depth of the layer and then compared to the distribution curves of the tornadic and nontornadic subsets. The large number of cases then began to show the signals of values that were more likely in certain ranges and depths of supercell environments.

The assigned soundings were binned according to their launch location and tornadic or nontornadic classification. Then distributions of lapse rates were plotted to visually determine the differences between the nontornadic and tornadic samples. Initially the entire data set was used in the tornadic comparisons, but upon further inspection it was found that there was a significant difference in geographic regional lapse rates so the Great Plains and Southeast soundings were analyzed separately. First the data sets were binned by distance into four subsets with a bin size of 50 km and a 0-1 km layer lapse rate was calculated for each sounding. This effectively isolated different ranges of the inflow environment so that the extent of homogeneity and any range-dependent thermodynamic differences between the regions could be determined while maintaining a constant lapse rate depth. Then the distance range was held constant at 0-100 km from the targeted storm, encompassing the near to mid-field environment so that the depth of the lapse rate layer could be modified to explore potential differences in thermodynamic gradients in shallower versus deeper layers. In accordance with the Coniglio and Parker (2020) analysis and to highlight depths of the other studies (Parker, 2012, 2014; Wade et al., 2018), four layer depths were selected (0-100 m, 0-250 m, 0-1 km, and 0-3 km). Two of the layers included (0-1 km and 0-3 km) are currently

used as forecasting parameters (Rasmussen, 2003; Coffey et al., 2019; Sherburn and Parker, 2014). The other two layers (0-100 m and 0-250 m) were chosen based on the finding of Coniglio and Parker (2020) that near-ground tornadic lapse rates were 2 K/km lower on average than nontornadic lapse rates. However, the robustness of this finding was not explored in Coniglio and Parker (2020), the focus of which was on the kinematics of supercell environments. Comparing the Coniglio and Parker (2020) data set with the Southeast data set compiled in this study at the four different layers and ranges utilized a large data set to explore how the low-level lapse rates of nontornadic and tornadic environments differ as sampled from observed soundings.

Several variables were considered when calculating the lapse rates of the nontornadic and tornadic environments. Temperature was initially chosen for the lapse rate values as it is a common variable used in forecasting. Differences in the Southeast and Great Plains lapse rates indicated that moisture might be a key difference, so virtual temperature and equivalent potential temperature were tested. The results from the moisture-dependent lapse rate variables did not have any benefits over the initial lapse rates, therefore air temperature was used when calculating the lapse rates to follow past studies (Wade et al., 2018; Coniglio and Parker, 2020) and one accepted forecasting variable .

In order to objectively analyze the differences between the nontornadic and tornadic subsets, the mean of the tornadic and nontornadic lapse rates in each of the compiled environments were calculated and compared. Then statistical significance testing was conducted to objectively compare the defined subsets. A statistical student's t-test was applied initially because the distributions of the Great Plains data sets were approximately normal, but several Southeast distributions were bimodal so a t-test was not a satisfactory method to test all of the distributions. As an alternative to the parametric t-test, a Kolmogorov-Smirnov (K-S) statistical significance test was conducted. The

K-S test is useful when data distributions are unknown (Massey, 1951) and there is a single independent variable (Lilliefors, 1967). In this study a two-sample K-S test was used to compare two subsets with one independent variable: the temperature lapse rate over a defined depth and at a defined range. A conservative bias in the statistical significance of the K-S test has been expressed in past studies (Crutcher, 1975; Steinskog et al., 2007). To address this, the p-values from the t-test conducted on the Great Plains subsets were compared with the K-S test p-values of the same subsets. The results were similar and both tests identified the same comparisons as statistically significant. Therefore the K-S test was conducted for all of the comparisons between the nontornadic and tornadic subsets in each domain and in the comparisons between the two geographic regions. A p-value of less than 0.05 would confirm that the distributions of the two defined subsets are statistically significantly different from one another and could be used to distinguish the two distributions.

Finally the thermodynamic profiles of the tornadic and nontornadic soundings within a 100 km range were compiled into one representative sounding to compare to simulation profiles, as in Parker (2012). While the Parker (2012) simulation profiles extended to 10 km above ground level (AGL), the focus of this study was in the low-level stability so only 0-3 km was considered here. In order to directly compare the profiles in (Parker, 2012), potential temperature was interpolated at 10 m intervals. Then the values were averaged at each height to calculate the representative profile which were then subjectively compared to the simulated profiles to determine if the simulated profiles adequately represented the observed environments.

## Chapter 3

### Results

The final data set analyzed in this study was composed of 667 soundings collected during 25 years of field campaigns across the southeast, Great Plains, and Midwest regions of the United States (Fig. 2.2). These soundings were launched at a range within 200 km in the inflow environment of supercell thunderstorms. Comparisons and statistical analysis were conducted using this large data set to better understand the low-level thermodynamic stability of supercell environments and potential differences between tornadic and nontornadic supercell environments to improve the predictability of such events.

A kernel density estimation (KDE) was used to take a first look at the total data set (Fig. 3.1). KDE is a smoothing method that uses kernels derived from the discrete data points to create a two-dimensional contoured map. This replaces scatter plots of data points to easily examine the difference between the nontornadic and tornadic distributions. In Fig. 3.1, the most common 0-1 km lapse rates for both tornadic and nontornadic soundings appear to be nearly identical at approximately -8 K/km, which is less than the dry adiabatic lapse rate (-9.8 K/km). Less variability in the tornadic lapse rate values is found, especially within 80 km of the supercell. The variability in lapse rate values also decreases for both nontornadic and tornadic soundings at distances greater than 125 km. This could be caused by a smaller sample size at the end of the data set, but also could indicate the threshold of the proximity and the spatial extent of the inflow environment (Potvin et al., 2010; Coniglio and Parker,

2020). The signals found were further dissected with distribution curves and statistical analysis.

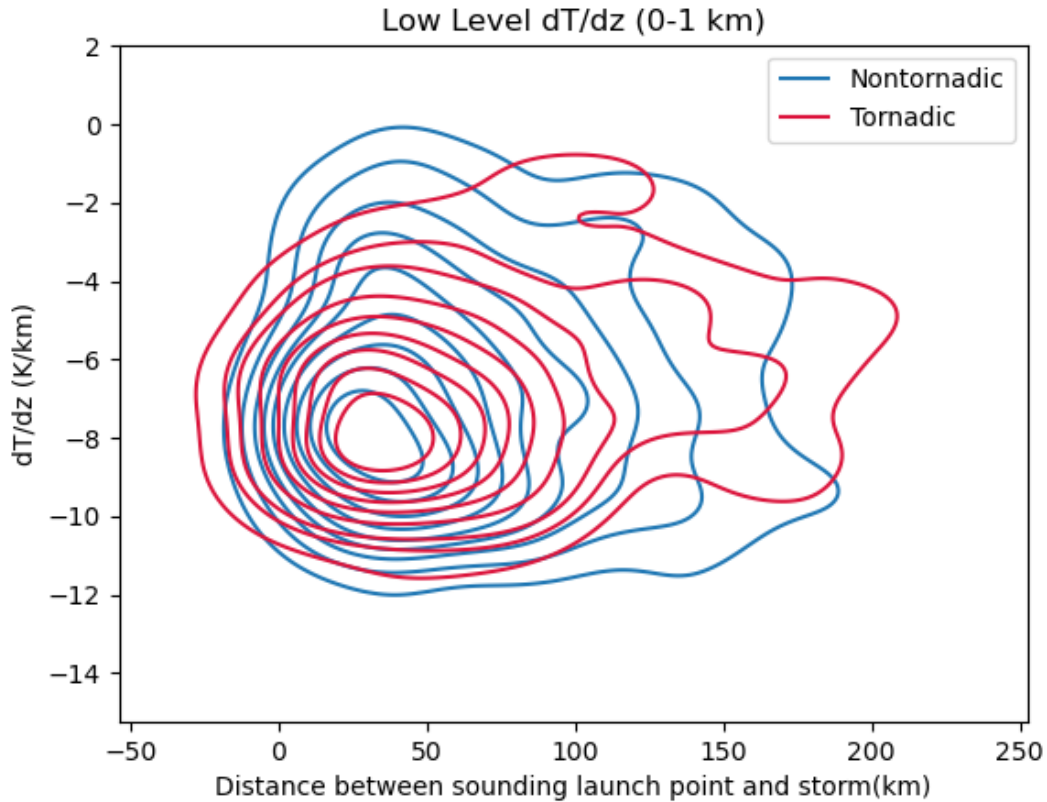


Figure 3.1: Kernel Density estimation (KDE) comparing the lapse rate values ( $dT/dz$ ) of all nontornadic (blue contours) and tornadic (red contours) soundings in the data set.

Since past studies (e.g., Bunkers et al., 2006; Murphy and Knupp, 2013) have noted that there are differences in Great Plains and Southeast convective environments, this data set was separated into four subsets (Great Plains (GP) tornadic soundings, Great Plains nontornadic soundings, Southeast (SE) tornadic soundings, and Southeast nontornadic soundings) to determine whether the geographic region played a significant role in the low level stability of supercell environments. As shown in Fig. 3.2, the

largest difference between the two regions is the mean 0-1 km lapse rate. Both the tornadic and nontornadic Great Plains subsets have a mean lapse rate value of -8 K/km while the tornadic and nontornadic Southeast subsets have a -5.5 K/km mean lapse rate. With a 2.5 K difference in mean lapse rates and large differences in sample sizes, the regions were analyzed separately in order to completely examine the differences of the tornadic and nontornadic supercell environments in each region.

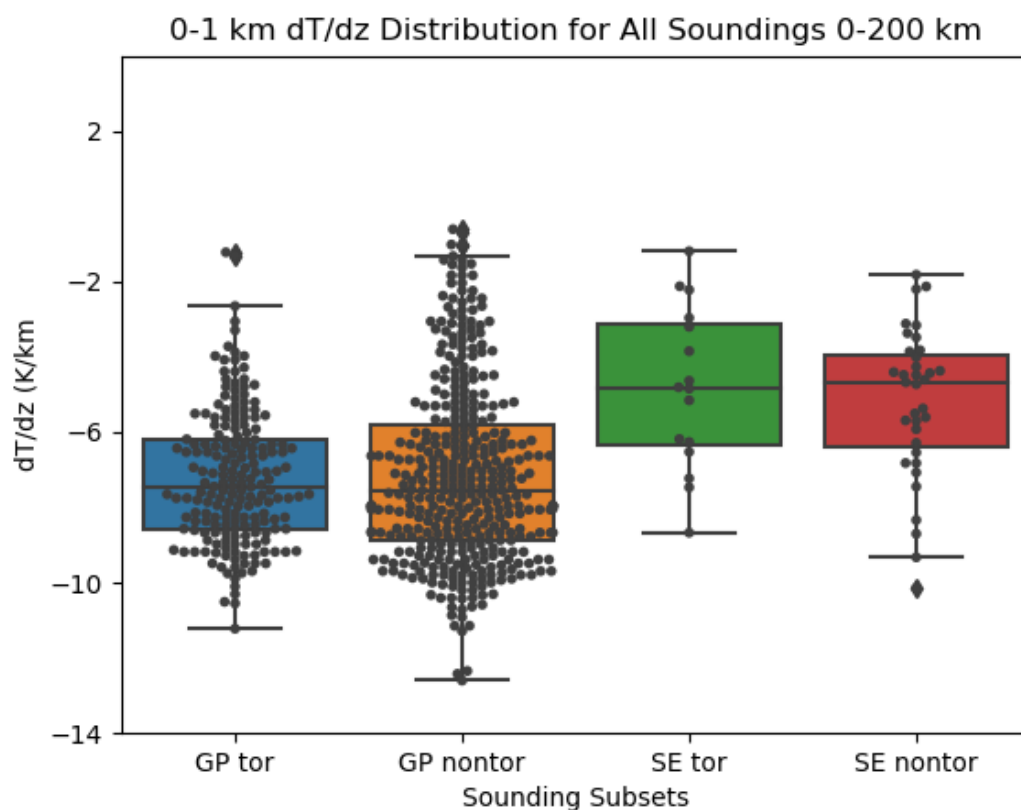


Figure 3.2: Box plots depicting low level stability (0-1 km  $dT/dz$ ) for each subset: Great Plains tornadic (blue), Great Plains nontornadic (orange), southeast tornadic (green), and Southeast nontornadic (red). The black points represent the lapse rate values of all data points in each subset.

## 3.1 Comparative Regional Analysis

Before each of the tornadic and nontornadic subsets was compared, an analysis of both regions in each inflow environment range was conducted to determine if any key features needed to be further examined. First soundings were binned based on both region and distance from the supercell mesocyclone. There were four binned distance subsets that each spanned a 50 km diameter within the inflow region as shown in Fig. 3.3. As was found in Fig. 3.2, the 0-1 km lapse rates in the Southeast are overall lower than the Great Plains lapse rates in each of the four subsets. This was most likely caused by soundings launched within stratiform precipitation or weak cellular convection within the inflow environment of supercells in the Southeast. Distribution maximums of each subset (Fig. 3.3) showed that the Great Plains 0-1 km lapse rate values are nearly dry adiabatic, though Fig. 3.3c has a secondary maximum of more stable lapse rates co-located with the Southeast distribution maximum.

The regional data set was also analyzed by binning the sounding profiles into four layers as shown in Fig. 3.4. This allowed for targeted analysis of potential differences in lapse rates that are found in the current forecast parameters (0-1 km lapse rate in Fig. 3.4c and 0-3 km lapse rate in 3.4d) as well as two additional shallow layers (0-100 m lapse rate in Fig. 3.4a and 0-250 m lapse rate in Fig. 3.4b) that have been analyzed in previous studies (e.g., Coniglio and Parker, 2020) but are not traditionally used in forecasting. As was with the distance binning in Fig. 3.3, the lapse rates in the Southeast are generally lower than the the lapse rates in the Great Plains data set. Also as the depth of the layer analyzed increases, the distribution maximum of each subset approaches the moist adiabatic lapse rate. This is not surprising as the lapse rate profile of the deeper layers reach and exceed the lifting condensation level (LCL). The 0-3 km layer (Fig. 3.4d) also has the greatest distribution maximum in lapse rate

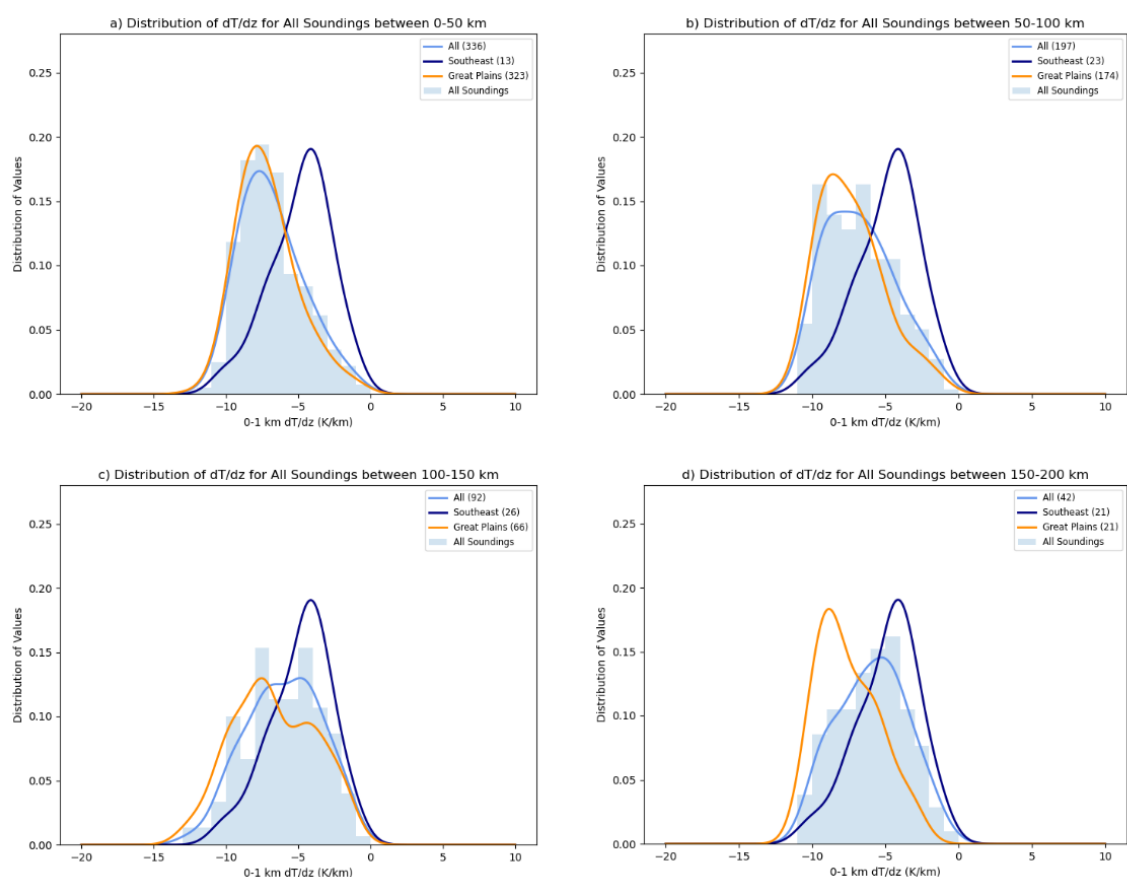


Figure 3.3: Histogram for all 0-1 km lapse rates (blue shading) and distribution curves for all 0-1 km lapse rates (light blue line), the Great Plains (orange line), and Southeast (navy line) data sets within a) 0-50 km of the supercell mesocyclone, b) 50-100km, c) 100-150 km, and d) 150-200 km.

values for both regions as the deeper profile also contains the least variability from top to bottom of the layer.

The two regions were then objectively compared at each binned distance and depth by conducting a two-sample K-S test. It was found that the difference between the distributions at all distances were statistically significant and also at all depths excluding the 0-100 m layer. Greater variability of temperatures within the 0-100 m layer likely resulted in the failed statistical significance test. The magnitude of the p-value



continued to decrease as the depth of the analyzed layer increased and variability was averaged out.

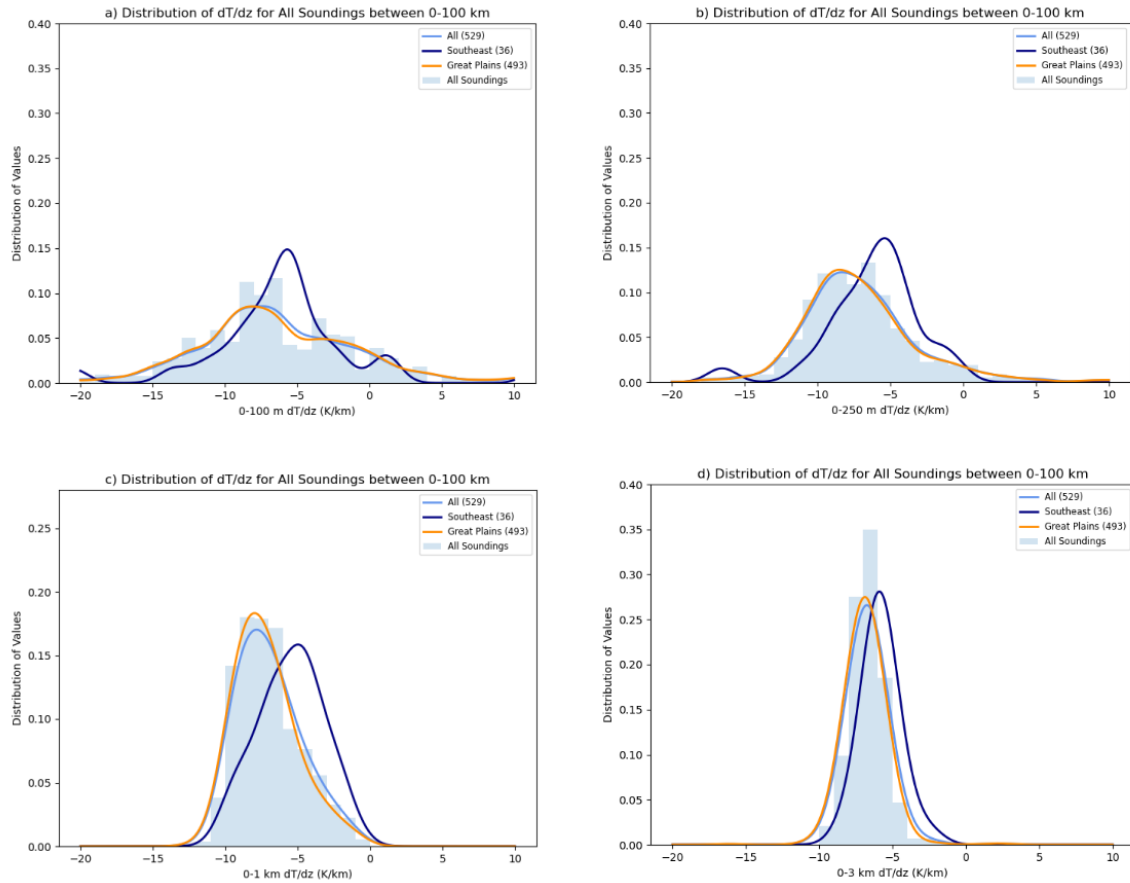


Figure 3.4: Histogram for all lapse rates (blue shading) and distribution curves for all lapse rates (light blue line), the Great Plains (orange line), and Southeast (navy line) data sets within 100 km of supercell updraft in a) 0-100 m, b) 0-250 m, c) 0-1 km, and d) 0-3 km layer depths.

## 3.2 Proximity Distributions

As shown in Fig. 3.2, each of the geographic regional data sets had a mean 0-1 km low-level lapse rate that was nearly equal between the respective tornadic and nontornadic subsets. This value was found by averaging all of the soundings that were launched

with 200 km of the updraft and is likely not representative of the entire supercell inflow environment. Therefore the soundings were binned into four subsets, each with a 50 km range, defined by distance to the supercell mesocyclone. The distributions of two subsets were compared with the same approach as the regional analysis and applied to the tornadic and nontornadic soundings of each geographic region.

### 3.2.1 Great Plains

The Great Plains data set contained 584 soundings binned into the four distance subsets with eighty-five percent of the soundings located within 100 km of the supercell. The distribution curves of the 0-1 km lapse rates binned between 0-50 km (Fig. 3.5a) and 50-100 km (Fig. 3.5b) are relatively similar to one another with the distribution maximums for both tornadic soundings and nontornadic lapse rates between -7.5 and -8.5 K/km. The mean tornadic lapse rates are slightly lower than the nontornadic lapse rates in each subset. There are more nontornadic soundings with lapse rate magnitudes lower than 4.5 K/km at all distances from the supercell. At further distances the distribution curves also begin to deviate from a normal to bimodal distribution. This is especially apparent in the nontornadic distribution curves between 100-150 km (Fig. 3.5c) and 150-200 km (Fig. 3.5d) with a second maximum in the stable lapse rate values between -4.5 to 0 K/km. The bimodal distribution could be a result of the smaller sample size at the greater ranges since only fifteen percent of the soundings were launched between 100-200 km from a supercell. The number of tornadic soundings with lapse rate magnitudes less than 4.5 K/km also dramatically decreases at all distances. These smaller tails, when compared to the nontornadic soundings in the distribution curves, exemplifies the lower variability in tornadic lapse rates shown in Fig. 3.1.

A K-S test was conducted comparing between the difference in the nontornadic and tornadic distributions of the Great Plains subset. There was only one statistically

significant range of the inflow environment (100-150 km from the supercell). The statistically significant difference is due to that the maximum of the tornadic distribution curve in 3.5 is less than the moist adiabatic lapse rate and in between the bimodal distribution peaks of the nontornadic subset. This could be noise from a small sample size, but is still worth noting. Nothing statistically significant can be confirmed from the other three binned Great Plains subsets.

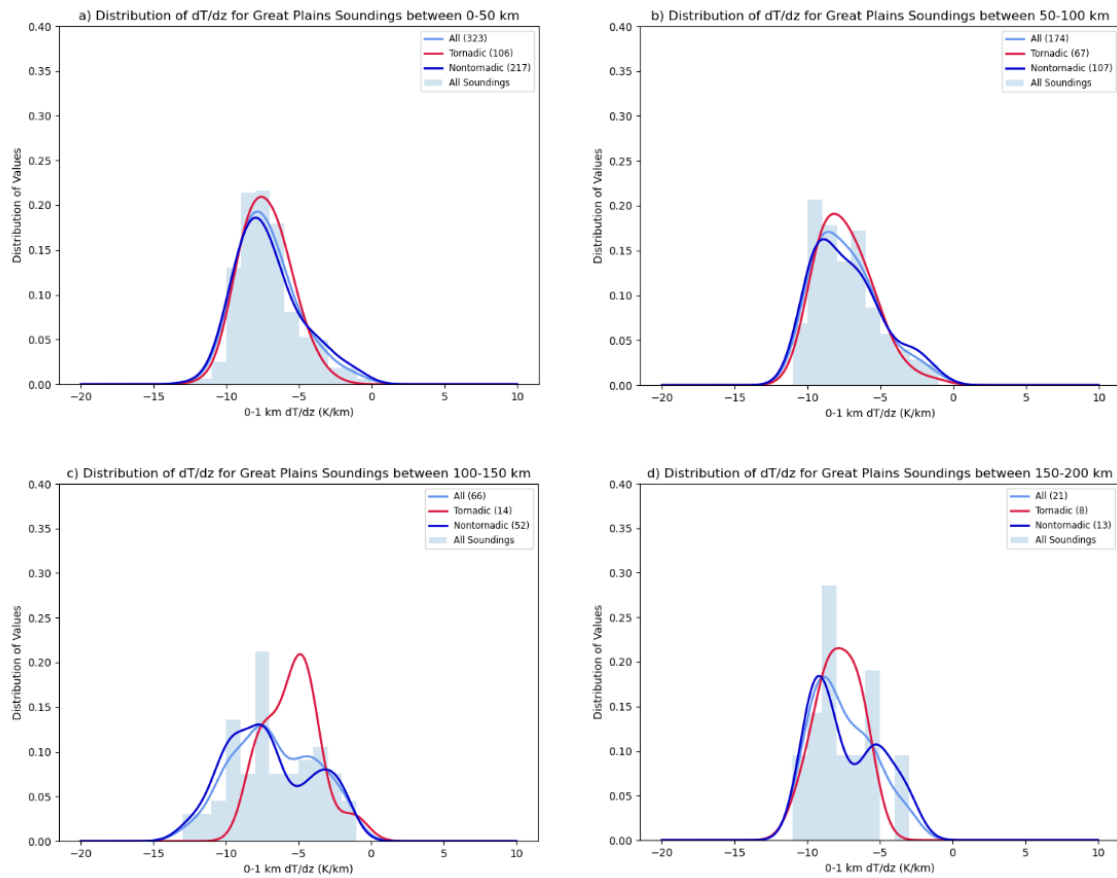


Figure 3.5: Histogram for all 0-1 km lapse rates (light blue shading) and distribution curves for all 0-1 km lapse rates (light blue line), the Great Plains nontornadic (blue line), and Great Plains tornadic (red line) subsets within a) 0-50 km of the supercell mesocyclone, b) 50-100km, c) 100-150 km, and d)150-200 km.

### 3.2.2 Southeast U.S.

The total Southeast data set contained 83 soundings binned into distance range subsets with the same criteria as the Great Plains soundings. Unlike the Great Plains distributions, five out of eight Southeast distribution curves in Fig. 3.6 have a bimodal distribution. The other three curves have a normal distribution. The bimodal distribution is most likely attributed to a small sample size of the subsets, but cannot be completely overlooked. Three peaks in the distributions of separate Southeast supercell subsets are found to occur near the dry adiabatic lapse rate, which deviates from the moist adiabatic lapse rate that has been more common in the overarching Southeast data set. This could be due to noise of a small sample size.

At closer distances, the lapse rate values of Southeast tornadic soundings appear to be more variable than nontornadic soundings as distribution maxima are noted near both the moist adiabatic lapse rate and dry adiabatic lapse rate within 50 km (Fig. 3.6a) and decreasing to nearly 0 K/km and the moist adiabatic lapse rate in the far-field (Fig. 3.6b and Fig. 3.6c). Meanwhile the nontornadic soundings in the same subsets peak near -5 K/km, similar to the mean lapse rate in Fig. 3.2. At the farthest range between 150-200 km (Fig. 3.6d), the tornadic distribution becomes less variable than the nontornadic distribution.

No lapse rate differences between the tornadic and nontornadic environments were found to be statistically significant at any range. This was not surprising as variability of both distributions is large within each subset and difficult to compare to one another.

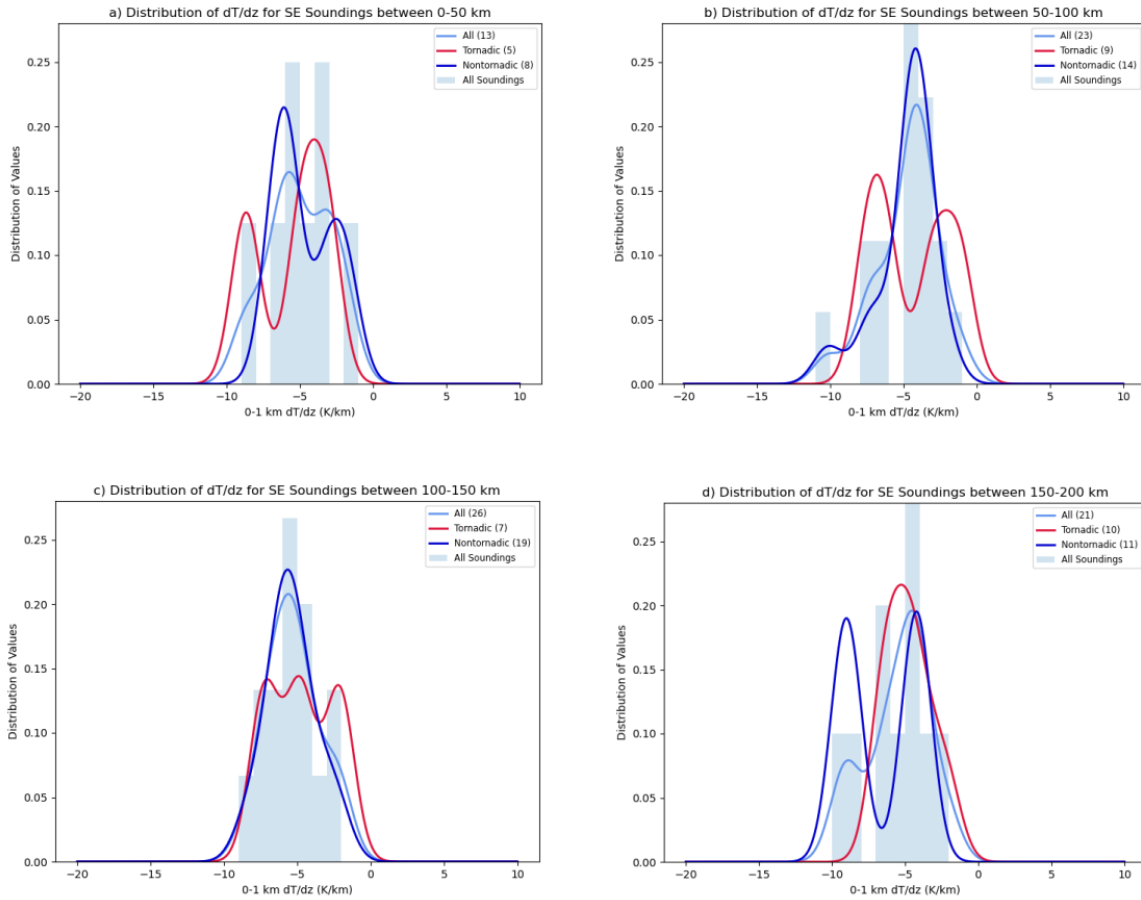


Figure 3.6: Same as Fig. 3.5, but for the Southeast data set.

### 3.3 Layer Depth Distributions

In addition to analyzing how 0-1 km lapse rates evolve over different ranges in tornadoic and nontornadoic supercell inflow environments, it is imperative to also analyze the lapse rates within different vertical layers. This allows for the sampling of potential range-dependent heterogeneities as well as determining if other layers than the accepted 0-1 km and 0-3 km would be beneficial in forecasting tornadoic supercells. The two additional layers selected are 0-100 m and 0-250 m that were also used in the Coniglio and Parker (2020) study. The soundings analyzed in both regions contained those

launched within 100 km of the supercell mesocyclone to capture the near to mid-field environment.

### 3.3.1 Great Plains

With a set range of 100 km from the supercell mesocyclone, 493 soundings were included in the Great Plains data set. The first apparent difference between the layers in Fig. 3.7 is that the width of the distribution decreases as the depth of the layer increases. That is, the ranges of lapse rate values recorded increases substantially from the 0-3 km layer (Fig. 3.7d) to the 0-100 m layer (Fig. 3.7a) for both the tornadic and nontornadic sounding subsets. This mirrors the comparison of the two different geographic regions in Fig. 3.4d. Turbulence in the boundary layer that causes thermodynamic mixing likely increases the variability of the lapse rate values and decreases the distribution maximum in the shallow layers. In addition, the tornadic soundings have slightly lower lapse rate values in the 0-1 km (Fig. 3.7c and 0-3 km 3.7d layers which agrees with the finding from the previous section. There continues to be a signal of more nontornadic profiles with lapse rates between -4.5 and 0 K/km than tornadic profiles in the 0-100 m (Fig. 3.7a) and 0-1 km (Fig. 3.7c) layers.

The K-S test was also applied to the Great Plains subsets and differences between the nontornadic and tornadic distributions in the 0-3 km layer was found to be statistically significant with a p-value of 0.0127. To note, the subjective difference in distributions in the 0-3 km layer does not appear to be greater than the 0-1 km environment.

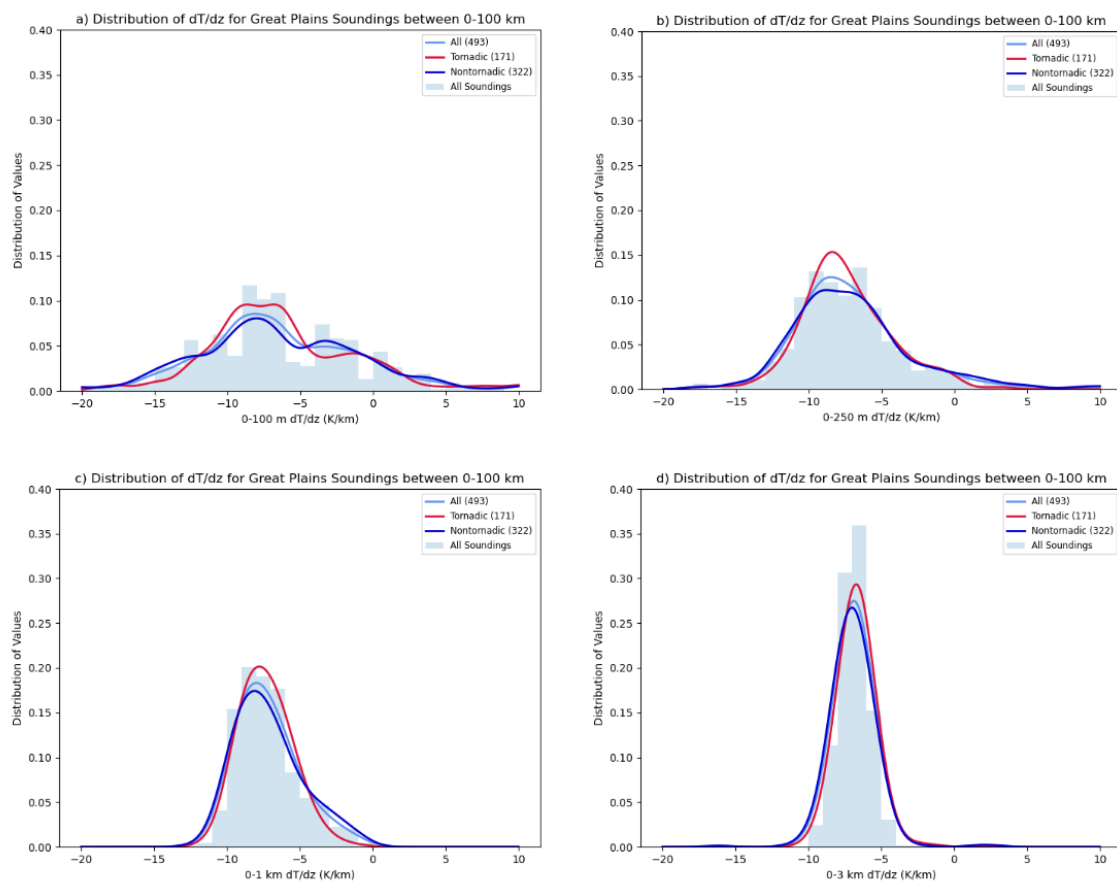


Figure 3.7: Histogram for all lapse rates (light blue shading) and distribution curves for all lapse rates (light blue line), the Great Plains nontornadic (blue line), and Great Plains tornadic (red line) subsets within 100 km of supercell updraft in a) 0-100 m, b) 0-250 m, c) 0-1 km, and d) 0-3 km layer depths.

### 3.3.2 Southeast U.S.

There were 36 soundings launched within 100 km of a supercell mesocyclone in the Southeast data set. Similarly to the Great Plains, the distribution maximum increases in the Southeast nontornadic subset as the depth of the layer analyzed increases (Fig. 3.8). Meanwhile the tornadic distribution curve in the 0-100 m layer (Fig. 3.8a) has a greater distribution maximum than the 0-250 m (Fig. 3.8b) and the 0-1 km (Fig. 3.8c) layers. In the same layer, the primary distribution maximum of the tornadic soundings occurs near the moist adiabatic lapse rate, but there is a second maximum

that falls within super adiabatic lapse rates and results in a bimodal distribution. Another bimodal distribution occurs in the 0-1 km layer (Fig. 3.8a) with maximums in the tornadic distribution curve near the dry adiabatic lapse rate and at roughly -2.5 K/km. All other distribution maximums in the subsets occur near the moist adiabatic lapse rate, which is expected. A K-S test was applied to the subsets and no statistical significant differences between the nontornadic and tornadic lapse rates in the Southeast subset were found in any of the layers.

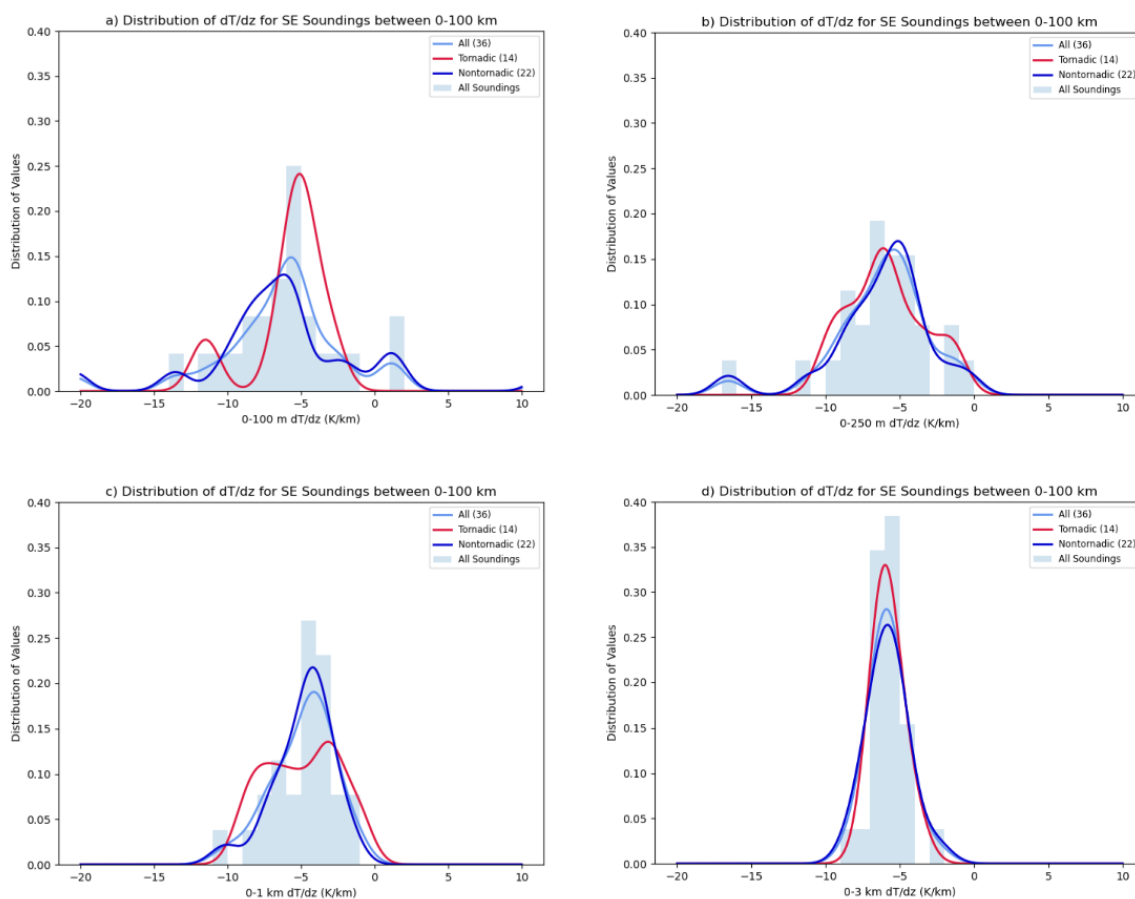


Figure 3.8: Same as Fig. 3.7, but for the Southeast data set.



### 3.4 Thermodynamic Profile Analysis

In order to understand how profiles simulated in past studies compare to profiles observed during field campaigns, potential temperature profiles were interpolated every 10 m using the Great Plains 0-100 km data set. Then the mean potential temperature of the nontornadic soundings and tornadic soundings was calculated at every level and plotted (Fig. 3.9). These averaged profiles were compared with the Parker (2012) simulation study to determine if any of the simulation profiles are representative of profiles in observed supercell environments.

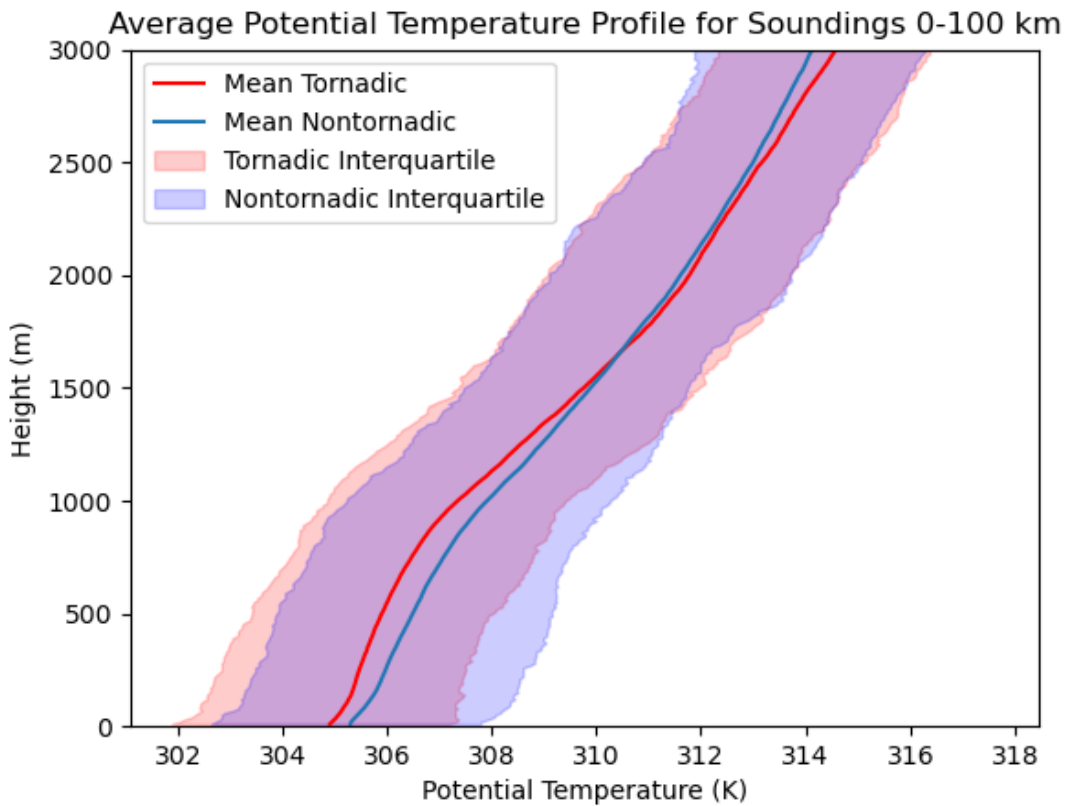


Figure 3.9: Averaged potential temperature profile for tornadic (red line) and non-tornadic (blue line) environments as well as each respective 25th to 75th percentile (shading).

First in the observed profiles, the 0-100 m tornadic profile is slightly more stable than the nontornadic profile as shown in Fig. 3.9, which is in agreement with the results above. Then both observed profiles follow nearly the same lapse rate to 1 km, though the tornadic profile is 2 K cooler than the nontornadic profile. Then from 1-2 km, the tornadic profile was more stable than the nontornadic profile with a potential temperature lapse rate 1 K/km greater than the nontornadic profile. Then the two profiles were nearly the same in potential temperature and lapse rate values from 2-3 km. In a subjective analysis, the 1-2 km layer has the greatest difference in thermodynamic stability between the nontornadic and tornadic profiles, but further analysis would need to be conducted to determine the extent of this difference.

In general the observed profiles appear to be more similar to one another than with any of the simulation profiles as shown in Fig. 3.10 and Fig. 3.11. The lapse rates between the observation and simulation tornadic profiles differ throughout the layer. Most notably, the observed tornadic profiles never reach a constant potential temperature, or dry adiabatic lapse rate, that Parker (2012) initiates in the ADIA, A3KM, and ALID simulation profiles. The simulation profiles also do not capture the changes in lapse rates at 100 m and 2 km that were present in the Great Plains data set. This is the result of a highly idealized simulation study and the profiles that were chosen. The comparison does not extend above 3 km as this study has focused on the low-level environment of supercells and to analyze the 0-3 km forecast parameter depth.

The comparisons between the nontornadic observation and simulation profiles are more similar than the tornadic ones. The average lapse rate of the observed profile is nearly equal to the BASE profile from the Parker (2012) study. Like the tornadic profiles, the changes in the observed lapse rates, particularly at 100 m and 2 km, are

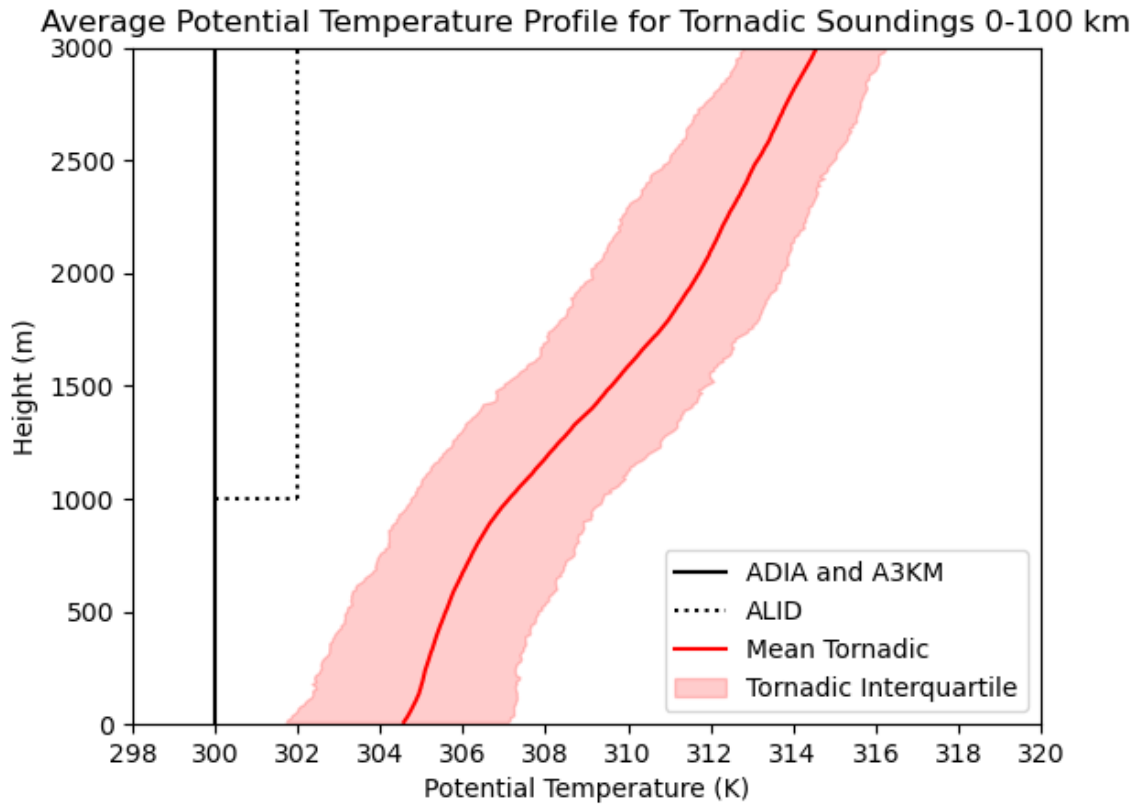


Figure 3.10: Averaged potential temperature profile for tornadoic environments (red line), the 25th to 75th percentile of the observed tornadoic profile (shading), and the Parker (2012) simulation profiles that intensify vortices: ADIA and A3KM (solid black line) and ALID (dotted black line).

not documented in any of the simulation profiles. These differences suggest that the Parker (2012) simulation profiles cannot be used to generalize the observed supercell environment.

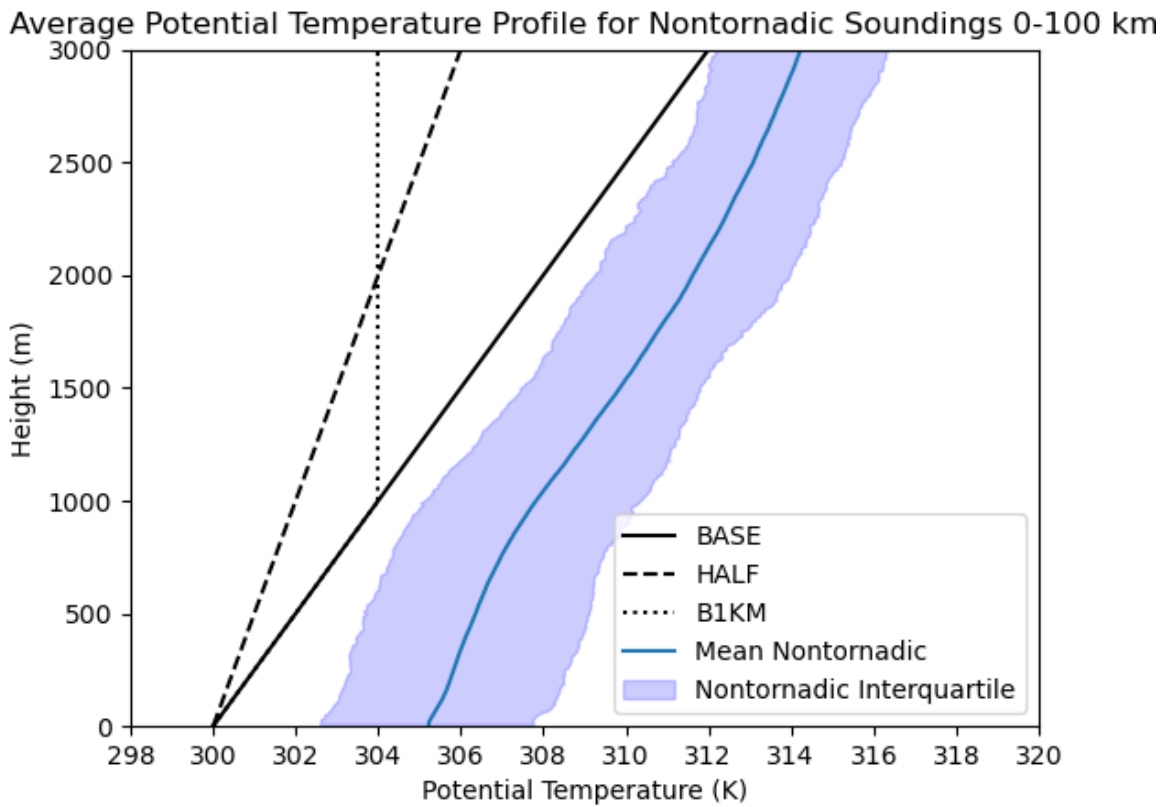


Figure 3.11: Averaged potential temperature profile for nontornadic environments (blue line), the 25th to 75th percentile of the observed nontornadic profile (shading), and the Parker (2012) simulation profiles that do not intensify vortices: BASE (solid black line), HALF (dashed black line), and B1KM (dotted black line).

## Chapter 4

### Discussion

In this study the distributions of over 600 nontornadic and tornadic soundings launched in supercell inflow environments were subjectively analyzed by comparisons of distribution curves for lapse rates. Then the same comparisons were analyzed objectively by conducting a K-S statistical significance test on the subsets. Finally thermodynamic profiles from the observed nontornadic and tornadic soundings were subjectively compared to simulation profiles. These comparisons led to a few new findings as well as a few expected outcomes.

#### 4.1 Supercell Environment Variability

A slight difference in lapse rate variability was first noted in Fig. 3.1, where the 0-1 km tornadic environments appeared to be less variable than the nontornadic environments. This was especially apparent in the soundings launched in the near-field (0-80 km) of the supercell inflow environment where the range of tornadic lapse rate values were roughly 2 K/km less than the nontornadic soundings. A second decrease in lapse rate variability for both data sets was found in the 100-200 km range. Inspection of the distribution curves of the Great Plains data set yielded similar results to the total data set. First the tornadic environments in the Great Plains showed less variability than nontornadic environments at each of the four binned ranges (Fig. 3.5). More importantly, there were more occurrences of lapse rates between -4.5 and 0 K/km that

were found in Great Plains nontornadic environments which expanded the variability of nontornadic environments.

Conversely there was more lapse rate variability in the tornadic Southeast supercell environments within 150 km of a supercell mesocyclone. The stability of the tornadic environments were less variable than the nontornadic environments at the 150-200 km binned range. In contrast to the Great Plains environments, there were more tornadic soundings with lapse rate values between -4.5 to 0 K/km than nontornadic soundings at distances greater than 50 km. The distribution maximum at more stable lapse rates in tornadic environments compared to the nontornadic environments in the Southeast could be caused by cloud cover and stratiform precipitation in the far-field inflow environment that typically did not occur in the Great Plains data set. The Coniglio and Parker (2020) climatology excluded all soundings launched within an outflow or precipitating region. Soundings launched in stratiform precipitation (less than 30 dBZ on WSR-88D radar base reflectivity scans) were included in the Southeast data set as Southeast events typically have stratiform precipitation within inflow environments.

These differences in where the maximum in lapse rate distributions occur for each geographical region were likely caused by the background environments of each region. Tornadic environments in the Southeast were, in general, more stable as was shown in Fig. 3.3 and Fig. 3.4. This did not completely explain the larger number of tornadic lapse rate values falling between -4.5 and 0 K/km in the Southeast (Fig. 3.6) the opposite occurring in the Great Plains environments (Fig. 3.5). This could be due to the higher surface relative humidity and lower LCLs in the Southeast compared to the Great Plains. Lower LCLs are indicative of higher surface relative humidity resulting in a more saturated layer and lower lapse rates. Therefore a more stable environment with lapse rate magnitudes less than 4.5 K/km may be more common in the Southeast environments. With the larger extent of convection surrounding the supercells in the

Southeast and lower instability than the Great Plains, there is a greater chance that tornadic environments may be stable farther from the supercell in the Southeast. The two regions did show that there are more nontornadic lapse rates with magnitudes of less than 4.5 K/km within 50 km of the supercell (Fig. 3.5a and Fig. 3.6a).

Overall the differences in the variability of the low-level lapse rates between the two regions is likely a cause of the large difference in sample size of the two subsets. There are 501 more Great Plains soundings than Southeast soundings and the sample size of each subset changes greatly at each range. There does appear to be more variability at ranges with smaller sample sizes and in the Southeast. The weight of each lapse rate value in the subsets with a smaller sample size is greater and therefore has a influence on the shape of the distribution curve. It is important to understand the extent that the significance of the smaller subsets can be trusted and what ultimately can be concluded from the results. Even with the smaller sample size, these subsets can still provide insight to the stability of tornadic and nontornadic environments, but the significance should be scrutinized.

## 4.2 Supercell Environment Stability

This study analyzed different ranges and depths of supercell inflow regions to address the disagreement of past findings (Parker, 2012, 2014; Wade et al., 2018; Coniglio and Parker, 2020). The largest contradiction in the previous studies was determining whether low-level tornadic or nontornadic supercell environments were more stable. A different set of parameters and thresholds defining each data set may have resulted in two separate conclusions so the Great Plains and Southeast data sets in this study were binned separately by distance and by vertical depth in order to determine where differences in the tornadic and nontornadic environments may arise.

Over all four distance ranges in the supercell inflow environment, this study found the 0-1 km tornadic lapse rates to be slightly more stable in both the Great Plains and the Southeast. This was evident in the distribution curves (Fig. 3.5 and Fig. 3.6) and mean lapse rate values. More notably, the tornadic soundings were also slightly more stable in the 0-100 m, 0-1 km, and 0-3 km layers in the both regions. These findings are consistent with the Coniglio and Parker (2020) results (0-100 m tornadic lapse rates are 2 K/km less than nontornadic lapse rates within the same region), though the mean lapse rate difference in this study was smaller than 2 K/km.

One possible explanation for slightly more stable tornadic soundings is anvil shading, studied extensively in the last decade. Nowotarski and Markowski (2016) found that in simulations anvil shading for supercells stabilizes the low-level environment, decreasing CAPE and the LCL height. The decrease in CAPE is expected as surface temperatures cool under the clouds. In addition to stabilizing the low-level environment, low-level shear increased in the inflow environment of the Nowotarski and Markowski (2016) simulation supercell. Both the lower LCL height and the heightened low-level shear created by the stabilization of the boundary layer may aid in tornado formation. Frame and Markowski (2010) did note that the orientation of the anvil shading to storm motion may inhibit the increase of low-level wind shear. The amount of anvil shading over the inflow environment could determine the magnitude of cooling and therefore the influence on low-level wind shear. The dependence of storm motion would agree with the slightly more stable tornadic soundings in the current data set not being statistically significant as the effect of anvil shading could change for each storm environment.



## 4.3 Statistical Analysis

Once the subsets were subjectively compared, a K-S statistical significance test was conducted to objectively determine whether any differences in the subset distributions may be statistically significant. Similarly to the initial distribution analysis, the K-S test was first applied to the geographic regional comparisons and then to the nontornadic and tornadic subset comparisons.

### 4.3.1 Regional Statistical Significance

Differences between the Great Plains and Southeast lapse rates were expected due to the difference in the mean lapse rate and maximum distribution values between the two regions. These differences proved to be statistically significant. An average 2.5 K/km lapse rate difference was found between the the Great Plains and Southeast caused by the background environments of the two regions. The differences in instability, low-level relative humidity, and the occurrence of widespread precipitation between the two geographical regions, among other factors, likely produced the statistically significant difference in the lapse rate distributions. The 0-100 m layer was the only layer that the Great Plains and Southeast lapse rate comparison was not statistically significant, likely because of the shallowness of the layer and the near-ground processes increasing the variability.

### 4.3.2 Comparing Tornadic and Nontornadic Subsets

The comparisons between tornadic and nontornadic subsets for the Southeast and Great Plains yielded little statistical significance. Of note, the 100-150 km range subsets in the Great Plains and the 0-3 km layer in the Great Plains were found to have statistically significant differences in the distributions of lapse rate values. The

maximum tornadic distribution magnitude was 3.5 K/km less than the maximum of nontornadic values in the 100-150 km range. The second category that passed the statistical significance test was the 0-3 km layer of the Great Plains data set. This was also the layer that resulted in the largest difference in mean lapse rate values between the tornadic and nontornadic subsets. The 0-3 km layer was the most expected to be statistically significant with lapse rates calculated over the largest depth and therefore excluding the greatest amount of variability. This resulted in nearly normal distribution curves for both the nontornadic and tornadic subsets in the Great Plains and Southeast. The 0-3 km lapse rate differences within the Great Plains data set were statistically significant, but was not the case in the Southeast data set. The discrepancy in the significance was most likely caused by regional differences, namely elevated mixed layers (EML), which are common during severe weather events across the Great Plains. EML base heights in the Great Plains are usually found around 700 mb (3.5 km) with a sharp inversion below the layer. The strength of this inversion modifies the 0-3 km lapse rate values as the temperature at the top of the layer is higher when an EML is present. Therefore slightly more stable lapse rates such as those found in the Great Plains tornadic subset could be due to this stronger inversion near the layer top (not explicitly examined for this study). Unlike the Great Plains, EMLs are not common at the same height across the Southeast and therefore does not influence the lapse rates. The lack of EML could increase the variability of the 0-3 km lapse rates in the Southeast and decrease the difference between the Southeast tornadic and nontornadic lapse rates.

The null hypothesis of no difference between the nontornadic and tornadic lapse rates could not be rejected when comparing each of the other subsets. This could be a product of the smaller sample sizes in the Southeast data set and smaller sample sizes

of the range binned subsets. It is also the result of variability of lapse rates within each layer analyzed.

## 4.4 Comparison of Observed to Simulation Profiles

The final step of the analysis was to create an observed average profile for all of the Great Plains tornadic and nontornadic soundings. This was done by calculating the potential temperature at each interpolation level and averaging and subjectively comparing the resultant profiles to the Parker (2012) simulation profiles. Before comparing the profiles it is important to note that there were four distinct levels within the first 3 km where the slope of the observed potential temperature profile changed: 100 m, 1 km, 2 km, and 3 km. The 0-1 km level has been accepted as a forecast parameter for severe weather, but substantial changes between the 0-100 m and 1-2 km layers are important to understanding if additional layers need to be considered for forecasting in the future. The potential temperature profiles of the both the nontornadic and tornadic observed soundings did not equal any of the simulation profiles. This was somewhat expected as initial conditions and parameterizations of the model are not exactly the same as each observed supercell environment. The Parker (2012) simulations were also highly idealized and assumed a dry environment near the profiles with dry adiabatic lapse rates. Therefore the simulation profiles did not represent the observed supercell environments in the Great Plains. The profiles also deviate even further from the Southeast low-level lapse rates as the mean Southeast lapse rates shown in the regional comparison are more stable than the Great Plains environments. Subjectively, the simulation profiles should not be used to define observed supercell environments, however a more objective comparison may emerge from future work.

# Chapter 5

## Conclusion

### 5.1 Summary

In this study, soundings launched during VORTEX-SE (2016-2019) were added to the Coniglio and Parker (2020) data set that compiled inflow soundings in supercell environments throughout 25 years of field campaigns. All of the VORTEX-SE soundings were quality controlled, assigned supercells, and flagged as tornadic or nontornadic following the same methodology as the initial data set. After expanding the proximity sounding range to 200 km from the supercell mesocyclone, a total of 667 soundings were included in the analyzed data set for this study, 584 of which from the Coniglio and Parker (2020) data set and 83 additional soundings from VORTEX-SE soundings. These soundings were compiled and analyzed to address two goals of the study: to examine whether tornadic supercell environments are more stable than nontornadic supercell environments in the lowest levels (Parker, 2014; Coniglio and Parker, 2020) or not (Parker, 2012; Wade et al., 2018) and determine if the (Parker, 2012) simulation profiles are representative of observed tornadic and nontornadic environments. A third goal was added to the study when it was found that the Great Plains and Southeast low level thermodynamic environments were significantly different: determine how general environmental differences in the two geographic regions may influence the stability of supercell environments.

The total data set was divided into multiple subsets in order to compare the tornadic and nontornadic lapse rates in inflow environments at four distinct ranges from the supercell for a 0-1 km lapse rate and four vertical layers for a range of 0-100 km. These subsets were selected based on the definitions of near and far-field ranges in previous studies and current forecast parameters. First, the subsets were subjectively compared by visually inspecting differences in lapse rate distributions between the Southeast and Great Plains data sets and then the nontornadic and tornadic soundings within each geographic region and category to address the first and third goals of this study. Then a K-S statistical significance test was conducted to objectively assess the differences that had been identified by subjectively comparing the distribution curves of the subsets. Finally the Coniglio and Parker (2020) data set was averaged to create a thermodynamic profile of all observed tornadic and nontornadic soundings within 100 km. These two profiles were individually compared to the Parker (2012) simulated profiles to address the second goal of the study. Overall it was found that there is not a significant difference in the low-level lapse rates of tornadic and nontornadic supercell inflow environments. Several additional conclusions were made:

- There is a statistically significant difference between Great Plains and Southeast lapse rates in the inflow environment of supercells for multiple ranges and depths analyzed.
- Tornadic lapse rate distributions follow a bimodal distribution in the Southeast data set rather than a normal distribution found in the Great Plains data set.
- Tornadic environments are slightly more stable in the 0-1 km layer than nontornadic environments at all ranges as well as the 0-100 m and 0-3 km layers in both the Great Plains and Southeast.

Thermodynamic lapse rates of Southeast supercell environments were on average 2.5 K/km lower than those of the Great Plains soundings and the difference between the Southeast lapse rates and Great Plains lapse rates was found to be statistically significant at all distances and all layers deeper than 100 m. This difference is caused by changes in the general environment of the geographical region that the sounding was launched. Surface relative humidity is typically higher in the Southeast than the Great Plains which causes observed lapse rates to be closer to the moist adiabatic lapse rate of 6.5 K/km instead of the dry adiabatic lapse rate. There was also stratiform precipitation noted in the inflow environment of supercells in the Southeast more often than the Great Plains cooling the temperature of at the surface. In addition, the bimodal distribution of most Southeast subsets compared to the normal distribution of the Great Plains subsets are most likely caused by the large difference between the two sample sizes.

The tornadic environments were found to be slightly more stable than the nontornadic environments in the Great Plains and Southeast at all ranges analyzed and within the 0-100 m, 0-1 km, and 0-3 km layers which is likely caused by storm-scale processes. This agrees with Coniglio and Parker (2020) finding in the 0-100 m layer. It also agrees with the 0-1 km Parker (2014) result. There were only two statistically significant categories when comparing the tornadic and non tornadic subsets, at the 100-150 km range and the 0-3 km layer in the Great Plains. These two subsets had the largest difference in mean lapse rate and also the least variability within the 0-3 km layer.

Averaged observed nontornadic and tornadic profiles were also compared to the Parker (2012) simulation profiles in an effort to determine if the simulation profiles are representative of tornadic and nontornadic supercell environments, but no definitive conclusions could be made. The simulation profiles were idealized and assumed a

dry adiabatic lapse rate that was not found in the observed profiles. The most notable difference between the nontornadic and tornadic profiles was found in the 1-2 km layer. This layer was not specifically accounted for in the simulation profiles and should be tested further to determine if it influences any vortex intensification in a model.

There are several limitations to conducting a study such as this. Soundings are a point observation and cannot be assumed to represent an entire inflow environment. In this case the use of a large data set accounts for and averages out some of the variability expected at different points within a supercell environment. In addition, analyzing the soundings within eight categories of a supercell environment binned by distance and depth also reduces the variability of the sounding lapse rates in that portion of the environment. The Southeast data set compiled for this study was also much smaller than the Great Plains data set. This could cause the signal of the smaller data set to get washed out if added to the larger data set. Significant differences were found between the Southeast and Great Plains data sets so the two regions were compared separately.

## 5.2 Future Work

This study analyzed the largest observed sounding climatology to date, but there was a significant difference in the sample size between the Great Plains and Southeast data sets. The next step to address this would be to add soundings launched during the Propagation, Evolution and Rotation in Linear Storms (PERiLS) field campaign conducted during spring 2022. While the field campaign focused on quasi-linear convective systems, several windsonds were launched within the inflow environment of supercells ahead of the the targeted convection. As field campaigns continue to be conducted,

this study can be easily revised to include additional soundings and create a larger data set for more robust analysis.

In addition to expanding the data set, the new soundings collected in 2022 and additional ones launched in the future could be used to test cases on the current data set. In order to do this, a piecewise linear function would need to be created from the averaged thermodynamic profile of the tornadic and nontornadic Great Plains data set and a second set of functions for the Southeast data set at defined ranges and depths. The new soundings would test the accuracy of the function to objectively analyze whether an environment is considered tornadic or not. If the piecewise function is accurate, it can be a tool to guide future thermodynamic studies of supercell inflow environments.

The initial phases of thermodynamic profile comparison between the observed soundings and simulated profiles yielded little similarities, so the differences could have big impacts on a resultant simulated vortex. First initializing the observed profiles in a model similar to Parker (2012) or a more recent scheme, then adding a set amount of wind shear and other parameters could aide in how modelled vortices form and evolve in different thermodynamic environments. Applying this data set directly to models is an excellent test of thermodynamic influence on convection and vortices in models to improve the understanding of how modelling handles the evolution of rotation in supercells.



## Reference List

- Anderson-Frey, A. K., Y. P. Richardson, A. R. Dean, R. L. Thompson, and B. T. Smith, 2019: Characteristics of tornado events and warnings in the southeastern united states. *Wea. Forecasting*, **34**, 1017–1034.
- Beebe, R. G., 1958: Tornado proximity soundings. *Bull. Amer. Meteor. Soc.*, **39**, 195–201.
- Bunkers, M. J., M. R. Hjelmfelt, and P. L. Smith, 2006: An observational examination of long-lived supercells. part i: Characteristics, evolution, and demise. *Wea. Forecasting*, **21**, 673–688.
- Chasteen, M. B., and S. E. Koch, 2022: Multiscale aspects of the 26–27 april 2011 tornado outbreak. part i: Outbreak chronology and environmental evolution. *Mon. Wea. Rev.*, **150**, 309–335.
- Coffer, B. E., and M. D. Parker, 2017: Simulated supercells in nontornadic and tornadic vortex2 environments. *Mon. Wea. Rev.*, **145**, 149–180.
- Coffer, B. E., and M. D. Parker, 2018: Is there a “tipping point” between simulated nontornadic and tornadic supercells in vortex2 environments? *Mon. Wea. Rev.*, **146**, 2667–2693.
- Coffer, B. E., M. D. Parker, R. L. Thompson, B. T. Smith, and R. E. Jewell, 2019: Using near-ground storm relative helicity in supercell tornado forecasting. *Wea. Forecasting*, **34**, 1417–1435.
- Coniglio, M. C., and M. D. Parker, 2020: Insights into supercells and their environments from three decades of targeted radiosonde observations. *Mon. Wea. Rev.*, **148**, 4893–4915.
- Crutcher, H. L., 1975: A note on the possible misuse of the kolmogorov-smirnov test. *J. Appl. Meteor.*, **14**, 1600–1603.
- Davies-Jones, R., 2015: A review of supercell and tornado dynamics. *Atmos. Res.*, **158**, 274–291.
- Frame, J., and P. Markowski, 2010: Numerical simulations of radiative cooling beneath the anvils of supercell thunderstorms. *Mon. Wea. Rev.*, **138**, 3024–3047.
- Guyer, J. L., and A. R. Dean, 2010: Tornadoes within weak cape environments across the continental united states. *25th Conf. on Severe Local Storms*.

- Lilliefors, H. W., 1967: On the kolmogorov-smirnov test for normality with mean and variance unknown. *J. Amer. Stat. Assoc.*, **62**, 399–402.
- Maddox, R. A., 1976: An evaluation of tornado proximity wind and stability data. *Mon. Wea. Rev.*, **104**, 133–142.
- Markowski, P., and Y. Richardson, 2010: *Mesoscale Meteorology in Midlatitudes*. Wiley-Blackwell, 430 pp.
- Massey, F. J., 1951: The kolmogorov-smirnov test for goodness of fit. *J. Amer. Stat. Assoc.*, **46**, 68–78.
- Murphy, T. A., and K. R. Knupp, 2013: An analysis of cold season supercell storms using the synthetic dual-doppler technique. *Mon. Wea. Rev.*, **141**, 602–624.
- Nowotarski, C. J., and P. M. Markowski, 2016: Modifications to the near-storm environment induced by simulated supercell thunderstorms. *Mon. Wea. Rev.*, **144**, 273–293.
- Parker, M. D., 2012: Impacts of lapse rates on low-level rotation in idealized storms. *J. Atmos. Sci.*, **69**, 538–559.
- Parker, M. D., 2014: Composite vortex2 supercell environments from near-storm soundings. *Mon. Wea. Rev.*, **142**, 508–552.
- Parker, M. D., 2021: Environmental evolution of long-lived supercell thunderstorms in the great plains. *Wea. Forecasting*, **36**, 2187–2209.
- Potvin, C. K., K. L. Elmore, and S. J. Weiss, 2010: Assessing the impacts of proximity sounding criteria on the climatology of significant tornado environments. *Wea. Forecasting*, **25**, 921–930.
- Rasmussen, E. R., 2003: Refined supercell and tornado forecast parameters. *Wea. Forecasting*, **18**, 530–535.
- Rasmussen, E. R., and D. O. Blanchard, 1998: A baseline climatology of sounding-derived supercell and tornado forecast parameters. *Wea. Forecasting*, **13**, 1148–1164.
- Rotunno, R., and J. Klemp, 1984: On the rotation and propagation of simulated supercell thunderstorms. *J. Atmos. Sci.*, **42**, 271–292.
- Schneider, R. S., A. R. Dean, S. J. Weiss, and P. D. Bothwell, 2006: Analysis of estimated environments for 2004 and 2005 severe convective storm reports. *23rd Conf. on Severe Local Storms*.
- Sherburn, K. D., and M. D. Parker, 2014: Climatology and ingredients of significant severe convection in high-shear, low-cape environments. *Wea. Forecasting*, **29**, 854–887.

- Showalter, A. K., and J. R. Fulks, 1943: Preliminary report on tornadoes. u.s. weather bureau.
- Smith, B. T., R. L. Thompson, J. S. Grams, C. Broyles, and H. E. Brooks, 2012: Convective modes for significant severe thunderstorms in the contiguous united states. part i: Storm classification and climatology. *Wea. Forecasting*, **27**, 1114–1135.
- Steinskog, D. J., D. B. Tjostheim, and N. G. Kvamsto, 2007: A cautionary note on the use of the kolmogorov–smirnov test for normality, low-cape convection. *Mon. Wea. Rev.*, **135**, 1151–1157.
- Thompson, R. L., C. M. Mead, and R. Edwards, 2007: Effective storm-relative helicity and bulk shear in supercell thunderstorm environments. *Wea. Forecasting*, **22**, 102–115.
- Thompson, R. L., B. T. Smith, J. S. Grams, A. R. Dean, and C. Broyles, 2012: Convective modes for significant severe thunderstorms in the contiguous united states. part ii: Supercell and qlcs tornado environments. *Wea. Forecasting*, **27**, 1136–1154.
- Wade, A. R., M. C. Coniglio, and C. L. Ziegler, 2018: Comparison of near- and far-field supercell inflow environments using radiosonde observations. *Mon. Wea. Rev.*, **146**, 2403–2415.
- Wade, A. R., and M. D. Parker, 2021: Dynamics of simulated high-shear low-cape supercells. *J. Atmos. Sci.*, **78**, 1389–1410.
- Wang, J., H. L. Cole, D. Carlson, E. R. Miller, K. Beierle, A. Paukkunen, and T. K. Laine, 2002: Corrections of humidity measurement errors from the vaisala rs80 radiosonde— application to toga coare data. *J. Atmos. Sci.*, **19**, 981–1002.
- Weckwerth, T. M., J. W. Wilson, and R. M. Wakimoto, 1996: Thermodynamic variability within the convective boundary layer due to horizontal convective rolls. *Mon. Wea. Rev.*, **124**, 769–784.